Neuron
Article

Hts/Adducin Controls Synaptic Elaboration and Elimination

Jan Pielage,[1,3,*] Victoria Bulat,[3] J. Bradley Zuchero,[2] Richard D. Fetter,[1,4] and Graeme W. Davis[1,*]
[1]Department of Biochemistry and Biophysics, University of California, San Francisco, 1550 4th Street, San Francisco, CA 94158, USA
[2]Department of Cellular and Molecular Pharmacology, University of California, San Francisco, San Francisco, CA 94158, USA
[3]Friedrich Miescher Institute for Biomedical Research, Maulbeerstrasse 66, 4058 Basel, Switzerland
[4]Present address: Howard Hughes Medical Institute, Janelia Farm Research Campus, Ashburn, VA 20147, USA
*Correspondence: jan.pielage@fmi.ch (J.P.), graeme.davis@ucsf.edu (G.W.D.)
DOI 10.1016/j.neuron.2011.02.007

SUMMARY

Neural development requires both synapse elaboration and elimination, yet relatively little is known about how these opposing activities are coordinated. Here, we provide evidence Hts/Adducin can serve this function. We show that *Drosophila* Hts/Adducin is enriched both pre- and postsynaptically at the NMJ. We then demonstrate that presynaptic Hts/Adducin is necessary and sufficient to control two opposing processes associated with synapse remodeling: (1) synapse stabilization as determined by light level and ultrastructural and electrophysiological assays and (2) the elaboration of actin-based, filopodia-like protrusions that drive synaptogenesis and growth. Synapse remodeling is sensitive to Hts/Adducin levels, and we provide evidence that the synaptic localization of Hts/Adducin is controlled via phosphorylation. Mechanistically, *Drosophila* Hts/Adducin protein has actin-capping activity. We propose that phosphorylation-dependent regulation of Hts/Adducin controls the level, localization, and activity of Hts/Adducin, influencing actin-based synapse elaboration and spectrin-based synapse stabilization. Hts/Adducin may define a mechanism to switch between synapse stability and dynamics.

INTRODUCTION

It is well established that the developing nervous system requires the combined activities of synapse formation and elimination (Goda and Davis, 2003; Luo and O'Leary, 2005), and there is increasing evidence that this is also true for the maintenance of mature neural circuitry (Holtmaat and Svoboda, 2009; Xu et al., 2009). The molecular mechanisms that control synapse formation have been studied extensively and include modulation of the neuronal cytoskeleton, target recognition, synapse assembly, and stabilization (Luo, 2002; Goda and Davis, 2003; Datwani et al., 2009). The opposing mechanisms that disassemble synaptic connections are beginning to emerge and include modulation of growth factor signaling, the submembranous spectrin/ankyrin skeleton, cell adhesion and cellular mechanisms that dismantle the neuronal membrane (Luo and O'Leary, 2005; Nikolaev et al., 2009; Koch et al., 2008; Pielage et al., 2005, 2008; Watts et al., 2003; Massaro et al., 2009). In general these different molecular mechanisms are studied in isolation. Yet it is also clear that the phenomena of synapse formation and retraction can coexist within the terminals of single neurons (Walsh and Lichtman, 2003). The mechanisms that serve to balance synapse stabilization and elimination within a neuron to achieve and maintain precise patterns of neural connectivity remain unknown.

To date, relatively few molecular mechanisms have been uncovered that participate in both synapse formation and elimination. Any such signaling system might reasonably be a point of control to balance synapse growth and elimination. Growth factor signaling is a type of global regulation that coordinates synapse formation and elimination with neuronal size (Huang and Reichardt, 2001). However, much less is known about how a balance between synapse stability and growth might be organized and executed locally within a nerve terminal. Potential candidates include adaptive immune signaling (Datwani et al., 2009) and control of cell adhesion. Remarkably, local regulators of the actin and microtubule cytoskeletons capable of balancing growth and elimination have yet to be clearly defined. Here, we provide evidence that the actin-capping, spectrin-binding protein Adducin participates in both actin dependent synaptic growth and synapse stabilization. As such, Adducin may serve to coordinate these opposing activities that normally specify the shape, extent, and stability of the presynaptic terminal.

The vertebrate genome encodes the three closely related *adducin* genes *α-adducin*, *β-adducin*, and *γ-adducin* that form tetramers composed of either α/β- or α/γ-heterodimers (Matsuoka et al., 2000). Adducin is a key protein involved in the assembly of the sub-membranous Spectrin-actin network (Bennett and Baines, 2001). Adducins contain an N-terminal head domain, a neck domain, and a C-terminal tail domain that includes a conserved 22 amino acid MARCKS-related domain (high homology to myristoylated alanine-rich C kinase substrate protein) (Matsuoka et al., 2000). Studies using in vitro biochemistry have shown that Adducin tetramers can cap the fast growing ends of actin filaments (Kuhlman et al., 1996) and recruit Spectrin to the ends of these actin filaments (Bennett et al., 1988). The actin binding activity of Adducin has been mapped to the MARCKS domain (Li et al., 1998). In some systems,

the phosphorylation of conserved serine residues within the MARCKS domain by protein kinase C abolishes the actin capping and Spectrin recruiting activities of Adducin (Chen et al., 2007; Kuhlman et al., 1996; Matsuoka et al., 2000). Thus, Adducin represents a regulated link between dynamic actin filaments and the stabilizing activity of the spectrin skeleton.

Adducin is highly expressed in the vertebrate nervous system (Bennett et al., 1988; Seidel et al., 1995). It is present in axonal growth cones and is concentrated within both presynaptic nerve terminals and postsynaptic dendritic spines (Matsuoka et al., 2000; Seidel et al., 1995). High levels of phosphorylated Adducin have been observed in hippocampal dendritic spines suggesting that the actin-binding properties of Adducin could be regulated during morphological spine plasticity (Matsuoka et al., 2000). Consistent with this possibility, β-*adducin* knockout mice have impaired LTP, LTD, and learning deficits (Porro et al., 2010; Rabenstein et al., 2005). In addition, increased phosphorylation of γ-Adducin was observed during long-term synaptic facilitation in *Aplysia* (Gruenbaum et al., 2003).

The *Drosophila* genome encodes a single *adducin* homolog, encoded by the *hu-li tai shao* (*hts*) gene (Robinson et al., 1994; Yue and Spradling, 1992). In *Drosophila*, Hts/Adducin was first identified as an essential component of fusomes and ring canals that are required for normal oogenesis (Robinson et al., 1994; Yue and Spradling, 1992). In these tissues Hts/Adducin colocalizes with Spectrin and actin. Importantly, *Drosophila hts/adducin* encodes an isoform (Hts-M) that includes the highly conserved MARCKS domain required for actin binding (Petrella et al., 2007).

RESULTS

Drosophila hts/adducin encodes four potential isoforms that have been previously characterized during *Drosophila* oogenesis (Petrella et al., 2007). Importantly, two isoforms contain a conserved MARCKS domain at the C terminus that is essential for the association with spectrin and actin-filaments in vertebrates. We observe only the shorter, 718 amino acid long, isoform in larval brain (Figure 1B and data not shown) and have termed this isoform Hts-M (Add 1 in Petrella et al., 2007). This isoform shares 38% overall identity with vertebrate α-Adducin and 64% identity within the MARCKS domain (www.flybase.org; Blast NCBI). Importantly, the MARCKS domain in *Drosophila* Hts-M includes a highly conserved central serine residue that can be phosphorylated by PKC/PKA to modulate the actin-recruiting and spectrin-binding properties of Adducin in vertebrates (Matsuoka et al., 2000; Figure 1A).

The organization of the *hts* locus is shown in a schematic that includes the position of three molecularly defined mutations and a deficiency that we use in this study (Figure 1A; Petrella et al., 2007). In addition, two antibodies, Hts1B1 and Hts-M, are available that recognize unique epitopes within *Drosophila* Hts (Petrella et al., 2007; Zaccai and Lipshitz, 1996; Figure 1A). These antibodies were used to confirm and define the molecular nature of our mutant *hts* alleles and to analyze the presence of the Hts-M isoform at the neuromuscular junction (NMJ). Both antibodies clearly label the *Drosophila* neuromuscular junction. Staining is present in the presynaptic motor axons, throughout the postsynaptic muscle, and is also concentrated within the postsynaptic muscle membrane folds, termed the subsynaptic reticulum (SSR), that surround the NMJ (Figure 1C).

The P element insertion hts^{1103} completely eliminates immunostaining assayed in situ and on western blots of larval brains, demonstrating the specificity of these antibodies (Figures 1B and 1C). The hts^{W532X} mutation results in a premature stop codon and only a small amount of residual staining is detectable in the motor nerve when using the Hts1B1 antibody (Figure 1C); however, no protein can be detected on the western blot (Figure 1B). The $hts^{\Delta G}$ mutation results in a truncated but stable protein lacking the MARCKS domain since staining with the Hts-M antibody is eliminated, while staining with the Hts1B1 antibody is retained. These results are in accordance with prior analysis of the *hts* mutations in oocytes (Petrella et al., 2007).

Loss of Hts/Adducin Causes Synapse Retraction and Elimination

The integrity of the NMJ and of individual synapses within the NMJ can be analyzed by immunolabeling synaptic markers that reside pre- and postsynaptically (Eaton et al., 2002; Koch et al., 2008; Massaro et al., 2009; Pielage et al., 2005, 2006, 2008). At the wild-type NMJ, the active-zone associated protein Bruchpilot resides in precise apposition to clusters of postsynaptic glutamate receptors throughout the NMJ (Figure 2A). In addition, the presynaptic vesicle marker Synapsin and the presynaptic membrane marker anti-HRP are opposed throughout the NMJ by the postsynaptic marker Dlg (Budnik et al., 1996), which labels the SSR (Figure 2A and 2E). In *hts* mutant animals, by contrast, we observe large regions of NMJs where postsynaptic antigens are no longer opposed by presynaptic markers. Specifically, within a single NMJ, regions of the presynaptic nerve terminal are devoid of presynaptic Brp but retain postsynaptic glutamate receptor clusters. The regions of the presynaptic nerve terminal that lack Brp have a discontinuous, fragmented presynaptic membrane, whereas regions of the same NMJ that contain Brp have a normal, continuous presynaptic membrane (Figures 2A–2D). Consistent with conclusions made in prior publications using an identical assay, the loss of presynaptic antigens and the associated fragmentation of the presynaptic membrane identify sites of synapse disassembly (Eaton et al., 2002; Koch et al., 2008; Massaro et al., 2009; Pielage et al., 2005, 2008). Staining *hts* mutant animals with additional pre- and postsynaptic markers further supports this conclusion (see Figure S1B available online).

The frequency and severity of synapse retractions were quantified in wild-type and *hts* mutant animals. Wild-type animals show virtually no evidence of synapse retraction, and when it does occur the retractions only encompass one or two synaptic boutons (Figures 2E and 2F; WT retraction 3.3%, n = 120). By contrast, *hts* mutations have a large increase in both the frequency and severity of NMJ retractions (23%–53%, n > 100) both on muscle 4 and muscles 6/7 (Figures 2E, 2F, S8). In addition, the frequency and severity of this phenotype correlates well with the molecular nature of our mutant alleles with hts^{1103}/Df^{BSC26} representing a strong hypomorph or null combination and showing the most severe phenotype. It is worth noting that the $hts^{\Delta G}$ mutation, which results in a truncation before the C-terminal MARCKS domain, shows a significant increase in

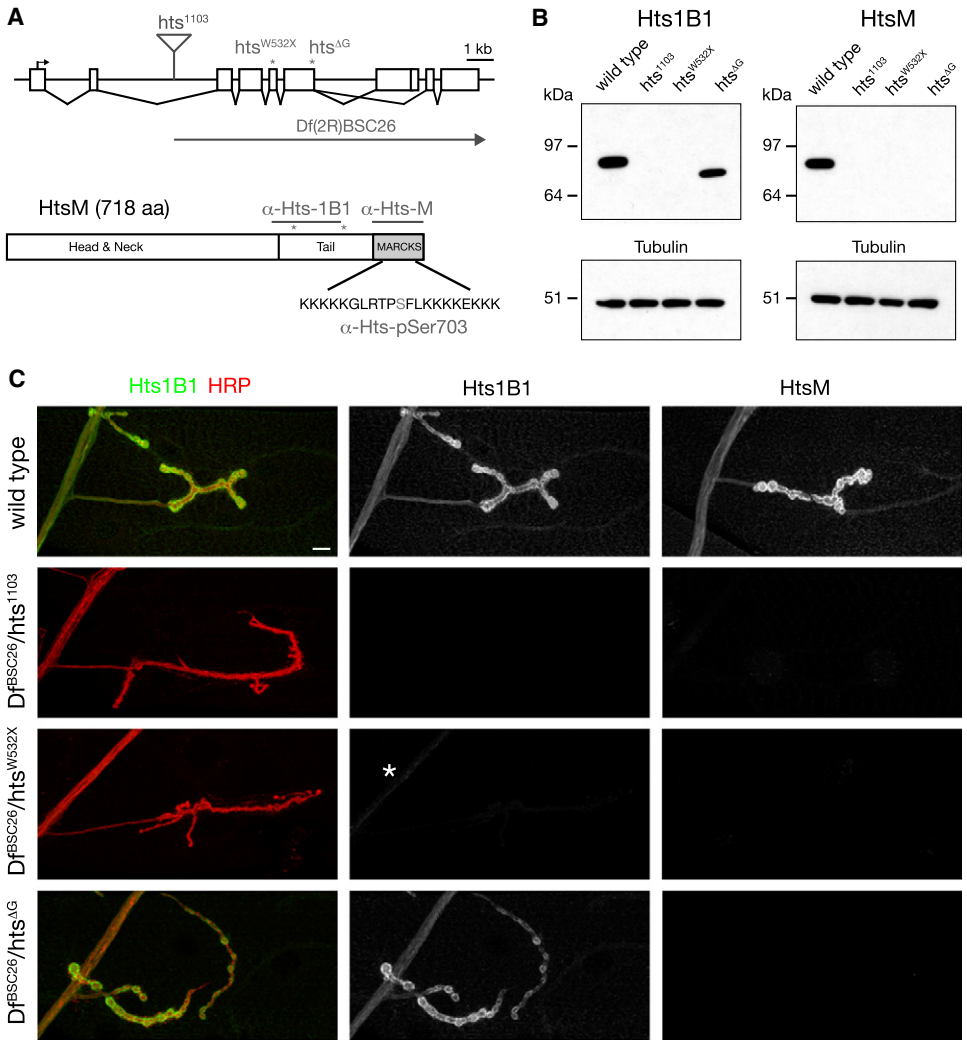

Figure 1. Hts-M Is Present Pre- and Postsynaptically at the *Drosophila* NMJ

(A) Schematic of the *Drosophila hts* locus. The position of the transposon and EMS-induced mutations are indicated (asterisks). The Hts-M isoform present at the *Drosophila* NMJ encodes a 718 aa long protein that contains a C-terminal MARCKS domain. Epitopes of the different Hts-M antibodies are indicated.

(B) Western blots of third-instar larval brain extracts. Anti-Hts1B1 and anti-Hts-M recognize single protein bands at approximately 80 kDa. The $hts^{\Delta G}$ mutation results in a truncated protein that can be detected using anti-Hts1B1 but not with anti-Hts-M.

(C) Analysis of Hts protein distribution at the *Drosophila* NMJ using the antibodies Hts-M and Hts1B1. In Df^{BSC26}/hts^{1103} mutant animals, no Hts1B1 or Hts-M staining can be detected. In Df^{BSC26}/hts^{W532X} mutant animals, small remnants of protein can be detected by the Hts1B1 antibody in the motoneuron axon (asterisk). In Df^{BSC26}/hts^{1103}mutant animals, significant amounts of Hts-M protein can be detected by Hts1B1; however, no protein can be detected with the Hts-M antibody.

NMJ retractions compared to wild-type, suggesting the importance of the Hts/Adducin actin-binding and capping activity for synapse stability (Figures 2E and 2F). However, the phenotype of the $hts^{\Delta G}$ mutation is not as severe as the null mutation. One possibility is that the truncated protein retains some actin-capping activity as indicated by in vitro studies (Li et al., 1998). Alternatively, there remains a stabilizing function that is independent of the MARCKS domain in vivo that is not predicted from the in vitro data. From these data, we conclude that Hts-M is required for the stabilization of the presynaptic nerve terminal. Adducin interacts with the Spectrin skeleton in *Drosophila* and other systems (Bennett and Baines, 2001). The demonstration that Hts/Adducin is necessary for synapse stability is consistent with prior studies demonstrating that presynaptic α-/β-Spectrin and the spectrin-interacting adaptor protein Ankyrin2 are required for synapse stability (Koch et al., 2008; Pielage et al., 2005, 2008). Indeed, the severity of synapse retraction and elimination is comparable in all three mutant genotypes. Consistent with this correlation, we observe a loss of the cell adhesion molecule Fasciclin II, the microtubule associated protein Futsch and Ankyrin2L (Ank2L) within retracting portions of the NMJ (Figures S1C–S1H). In addition, we observe that Ank2L staining is perturbed within stable regions of the NMJ (Figure S1H). Finally, loss of Hts/Adducin potentially has a minor impact on axonal

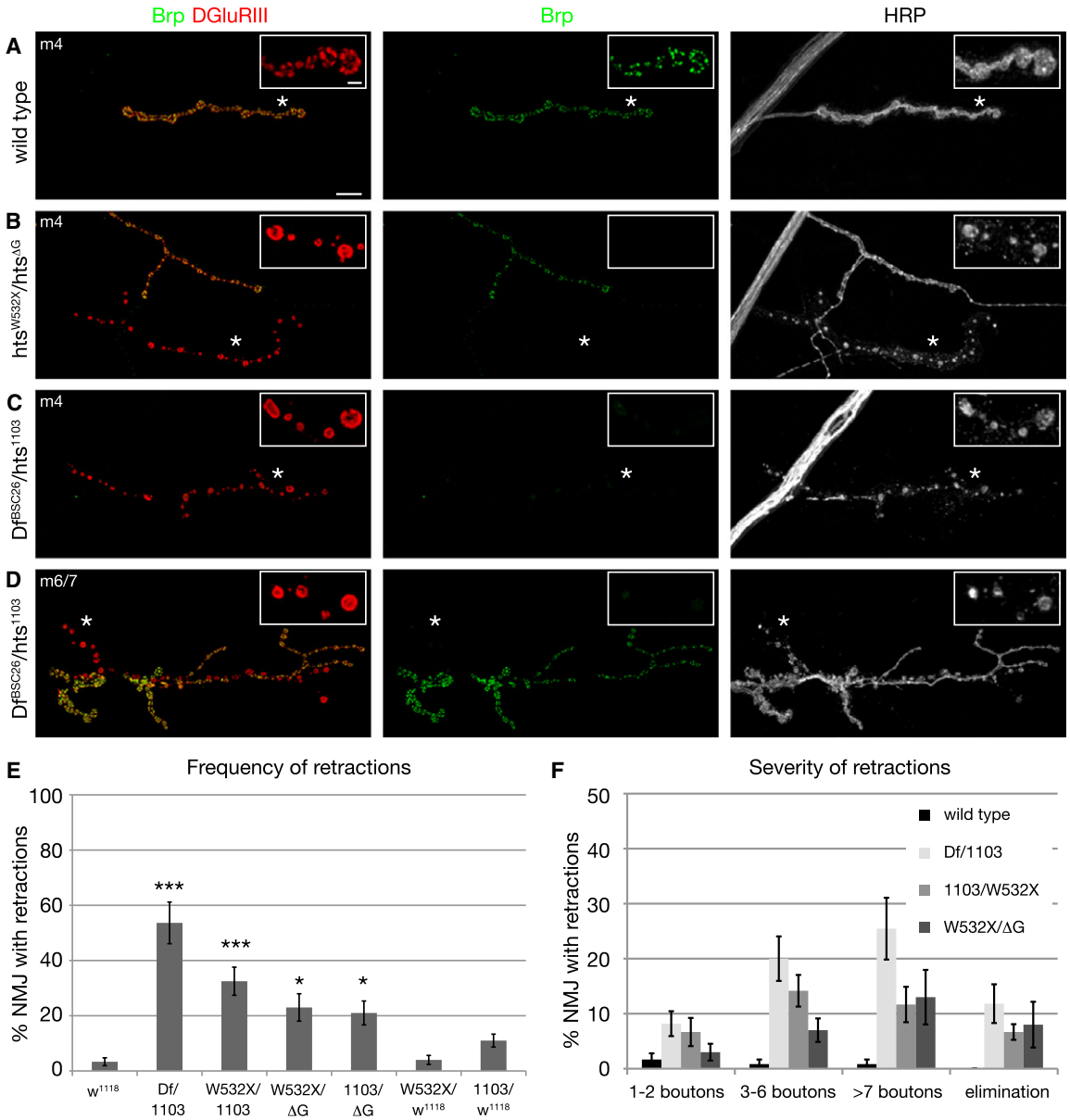

Figure 2. Mutations in *hts* Result in Severe Synaptic Retractions

(A–D) NMJs stained with markers for the presynaptic active zone protein Brp (green), postsynaptic glutamate receptors (DGluRIII, red), and the presynaptic membrane (HRP, white). The insets show individual channels at higher magnifications. (A) Wild-type (w^{1118}) muscle 4 NMJ. The presynaptic active zone protein Brp is found in perfect apposition to postsynaptic glutamate receptors. (B) A $hts^{W532X}/hts^{\Delta G}$ mutant muscle 4 NMJ. Two motoneurons innervate the muscle. One NMJ (asterisk) lacks all presynaptic Brp staining. The presynaptic membrane is fragmented and no longer continuous with the main motoneuron nerve. At higher magnification, it becomes evident that the glutamate receptor clusters appear fused and are no longer organized into distinct uniform clusters. (C) A Df^{BSC26}/hts^{1103} mutant muscle 4 NMJ. Only very small amounts of presynaptic Brp can be detected that are no longer organized into distinct puncta (asterisk). In addition, the presynaptic membrane is fragmented and discontinuous (asterisk) indicating the retraction of synapses. (D) A Df^{BSC26}/hts^{1103} mutant muscle 6/7 NMJ. At large parts of the NMJ the presynaptic marker Brp is absent although postsynaptic glutamate receptors are still present. The presynaptic membrane is fragmented at these sites (asterisk). Scale bar in (A) applies to (A)–(D) and represents 10 μm; insets 2 μm.

(E) Quantification of the frequency of synaptic retractions. All combinations of *hts* mutants show a significantly higher number of retractions compared to wild-type (n > 10 animals and > 100 NMJs each; *** indicates $p < 0.001$; * indicates $p < 0.05$; ANOVA). We do not observe significant numbers of retractions in hts^{W532X}/w^{1118} mutant animals, demonstrating that the observed phenotypes in $hts^{W532X}/hts^{\Delta G}$ are in part due to the lack of the MARCKS domain in the $hts^{\Delta G}$ mutation.

(F) Quantification of the severity of synaptic retractions. The severity was quantified based on the number of postsynaptic bouton profiles that lack the presynaptic marker Brp. Numbers represent percentage of total NMJs scored (n as in E). Elimination indicates the complete absence of distinct Brp signal and the complete fragmentation of the presynaptic membrane from one motoneuron innervation site (examples in B and C). Error bars represent SEM.

See also Figures S1 and S2.

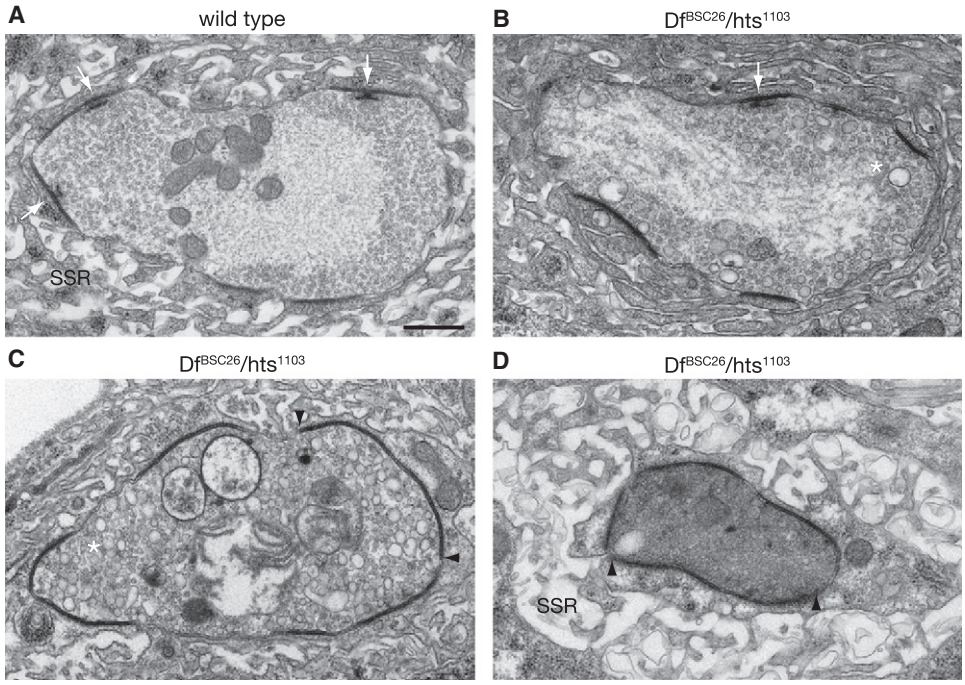

Figure 3. Ultrastructural Analysis of Synapse Retraction

(A) A bouton of a wild-type muscle 4 NMJ. Electron dense membranes indicate individual release sites (synapses). At multiple synapses presynaptic T bars are visible (white arrows). The presynaptic vesicles are uniformly distributed within the presynaptic bouton. The postsynaptic SSR is organized into distinct membrane folds.

(B–D) Representative examples of three different Df^{BSC26}/hts^{1103} mutant NMJs are shown. (B) In addition to normal synaptic vesicles, larger presynaptic vesicles become apparent (asterisk) at Df^{BSC26}/hts^{1103} mutant NMJs. Only one T bar is present at a synapse (white arrow). (C) Larger diameter vesicles are present throughout the presynaptic bouton (asterisk). No T bars are present, and the area of individual electron dense regions is increased (boundaries marked by arrowheads). (D) Presynaptic organelles or vesicles can no longer be identified. Almost the entire membrane of the bouton is electron dense. In addition, the postsynaptic SSR is no longer organized into compact membrane folds.

Scale bar in (A) applies to (A)–(D) and represents 500 nm. See also Figure S3.

transport. In *hts* mutant animals, we observe increased levels of synaptic antigens in the axon. However, the overall organization of the axonal cytoskeleton is not impaired (Figure S2A). The potential axonal transport defect is less severe than that observed in mutations in *ank2* or after presynaptic knockdown of the spectrin cytoskeleton (Figure S2B; Pielage et al., 2005; Koch et al., 2008). We propose that Hts/Adducin is required to maintain the stability of the spectrin-Ankyrin skeleton, previously shown to be required for NMJ stability (Pielage et al., 2005, 2008).

Altered Glutamate Receptor Clustering at Sites of Synapse Disassembly

During our analysis of NMJ disassembly, we observed an interesting change in postsynaptic glutamate receptor staining in regions of synapse retraction in *hts* mutant animals. In wild-type, as shown previously, glutamate receptors are organized into discrete clusters within the area of a synaptic bouton (Figure 2A, inset). By contrast, at sites of synapse retraction that show fragmentation of the presynaptic membrane, the glutamate receptor clusters appear confluent (Figures 2B–2D, insets). These receptors are no longer opposed by presynaptic Brp suggesting that they lack a functional presynaptic active zone. We speculate that the altered organization of postsynaptic glutamate receptor clusters could reflect a feature of ongoing synapse disassembly and degeneration, possibly reflecting the loss of *trans*-synaptic integrity (Eaton et al., 2002).

Ultrastructural Analyses

We next examined the NMJ of *hts* mutant animals at the ultrastructural level. A cross-section through a wild-type synaptic bouton is shown in Figure 3A. The synaptic bouton contains synaptic vesicles that are concentrated near electron dense active zones that include characteristic, electron dense presynaptic T bars (white arrows). The bouton is surrounded by complex muscle membrane folds (SSR). We sectioned NMJs of three different Df^{BSC26}/hts^{1103} mutant animals and present representative images of the retraction phenotype. We observe the appearance of abundant vacuoles within the presynaptic terminal (Figures 3B and 3C). The presence of vacuoles was previously associated with synapse retraction in *dynactin*, *spectrin*-RNAi, and *ankyrin2* mutant backgrounds (Eaton et al., 2002; Pielage et al., 2005, 2008). We also observe the expansion of the electron dense membrane domains that are typically associated with active zones. These enlarged electron dense domains do not contain T bars (Figures 3C and 3D). This is consistent with our light level analysis using the T-bar-associated protein

Brp as a marker for presynaptic active zones and glutamate receptor antibodies as a marker for the postsynaptic density (Kittel et al., 2006; Wagh et al., 2006). At retracting nerve terminals, Brp is absent, and we observe enlarged confluent domains of glutamate receptor staining (Figures S3A and S3B). To further address whether the enlarged electron densities might represent the enlarged glutamate receptor fields, we quantified glutamate receptor fields at the light level, comparing stable synapses (box 1 in Figure S3B) to retracting synapses (box 2 in Figure S3B) on the same muscle. This analysis reveals a significant 6-fold increase in the volume of glutamate receptor clusters and a corresponding 4-fold decrease in the number of separable glutamate receptor clusters per synaptic bouton. These data are consistent with the observation of nearly continuous electron dense regions in our EM analysis (Figures 3C and 3D). In addition, in sections where there appears to be a severe perturbation of presynaptic ultrastructure, we observe two additional phenotypes: (1) the postsynaptic SSR is less dense, consistent with the disassembly of the postsynaptic SSR as observed previously (Figure 3D; Eaton et al., 2002; Pielage et al., 2005), and (2) the presynaptic mitochondria are severely perturbed even though muscle mitochondria, in the same image, appear normal. Finally, in all cases, boutons with wild-type ultrastructure were also observed within each animal, consistent with our light level observations (data not shown). Thus, our ultrastructural data are consistent with the conclusion that *hts* is necessary to maintain the stability of the *Drosophila* NMJ.

Neuronal Hts Is Required to Maintain NMJ Stability

We next sought to define where Hts is required for synapse stability. First, we expressed transgenically encoded RNAi under UAS control (hts^{RNAi}) to knock down Hts protein in either the presynaptic neuron or postsynaptic muscle. Presynaptic expression of hts^{RNAi} significantly depletes Hts-M protein from the nervous system (Figure 4H). When hts^{RNAi} is expressed presynaptically, with or without coexpression of *dicer2* to enhance RNAi efficiency (Dietzl et al., 2007), we observe a significant increase in NMJ retractions compared to control (Gal4-driver lines crossed to w^{1118}) (Figures 4B and 4G; 36% and 28% of muscle 4 NMJs show retractions compared to 1% in control; n > 98 NMJs for all genotypes). In addition, presynaptic knockdown of Hts shows all hallmarks of synapse retraction observed in *hts* mutants including loss of presynaptic antigens, persistence of postsynaptic antigens (note the confluence of glutamate receptor staining as documented above; Figure 4B, inset) and the fragmentation of the presynaptic nerve membrane (Figure 4B; see below for additional quantification of bouton numbers). By contrast, although muscle-specific expression of hts^{RNAi} was equally efficient at eliminating Hts protein (data not shown), it did not cause an increase in synapse retractions (Figures 4C and 4G; 2% of NMJs show retractions, n = 60). In addition, the morphology of the NMJ appears grossly normal following postsynaptic knockdown of Hts (Figure 4C; see below for further quantification).

To further address the tissue-specific function of Hts, we expressed an *hts* cDNA in the *hts* mutant background using the GAL4/UAS expression system. We used a cDNA encoding the 718 aa long isoform of Hts that contains the conserved C-terminal MARCKS domain (*Hts-M*). The MARCKS domain containing isoform is the major Hts isoform expressed in the larval nervous system as wild-type Hts-M and UAS-expressed Hts-M protein run at equal sizes on western blots of larval brains (see below). We do not detect the OvHts isoform (1156 aa) that is present in nurse cells and oocytes (Petrella et al., 2007; data not shown). We find that presynaptic expression of *Hts-M* using *elav*-GAL4 in the *hts* mutant background (Df^{BSC26}/hts^{1103}) rescues the presynaptic retraction phenotype (Figures 4D and 4F; retraction frequency 7% compared to 54% in mutant animals, n > 98 NMJ). Importantly, this presynaptic rescue assay allows us to visualize Hts-M protein that is present in the presynaptic nerve terminal because we only resupply the protein in the motoneuron, not in the muscle. Hts-M protein is present within the presynaptic nerve terminal where it localizes at or near the presynaptic membrane but is not present within active zones marked by Brp (Figure 4E). In contrast, postsynaptic expression of *Hts-M* causes a slight, though not significant, reduction in the frequency of synapse retraction. However, we find that ectopic expression of Hts-M in muscle severely disrupts muscle and NMJ morphology (Figure S4). Thus, is it not possible to accurately quantify the postsynaptic contribution of *Hts-M* to NMJ stability when it is expressed via UAS-GAL4. From these data, both RNAi-mediated Hts knockdown and transgenic rescue, we conclude that Hts is required presynaptically to stabilize the NMJ.

Electrophysiological Analysis of Synaptic Transmission

We next analyzed synaptic transmission, comparing wild-type with the hts^{1103}/Df^{BSC26} allelic combination and with animals expressing hts^{RNAi} in presynaptic neurons. We find a significant increase in the average quantal amplitude in the hts^{1103}/Df^{BSC26} mutant animals and a corresponding decrease in average quantal content (Figures S5A–S5C). However, the increased mepsp amplitude was not observed in animals expressing hts^{RNAi} presynaptically. This could be due to a less severe knockdown of Hts protein. Alternatively, the increased average mepsp amplitude could reflect a postsynaptic activity of Hts. This possibility is consistent with the prior demonstration that knockdown of postsynaptic spectrin causes a comparable increase in quantal size (Pielage et al., 2006). We also find that synaptic transmission is considerably more variable in *hts* loss of function animals (Figure S5D). We plotted average mepsp versus average quantal content for individual NMJ recordings. There is more variation both in mepsp amplitude and quantal content compared to wild-type. This is consistent with prior studies demonstrating highly variable recordings at NMJ undergoing retraction (Massaro et al., 2009; Pielage et al., 2005, 2008). The observed increase in release variability is less severe than after knockdown of α-/β-*spectrin*, which might be accounted for by enhanced NMJ growth that is unique to *hts* mutant animals (see below). Together, these data indicate that Hts/Adducin does not have a strong, direct influence on either spontaneous or evoked vesicle release. The small changes in transmission that we observe are likely to be secondary to changes in NMJ morphology.

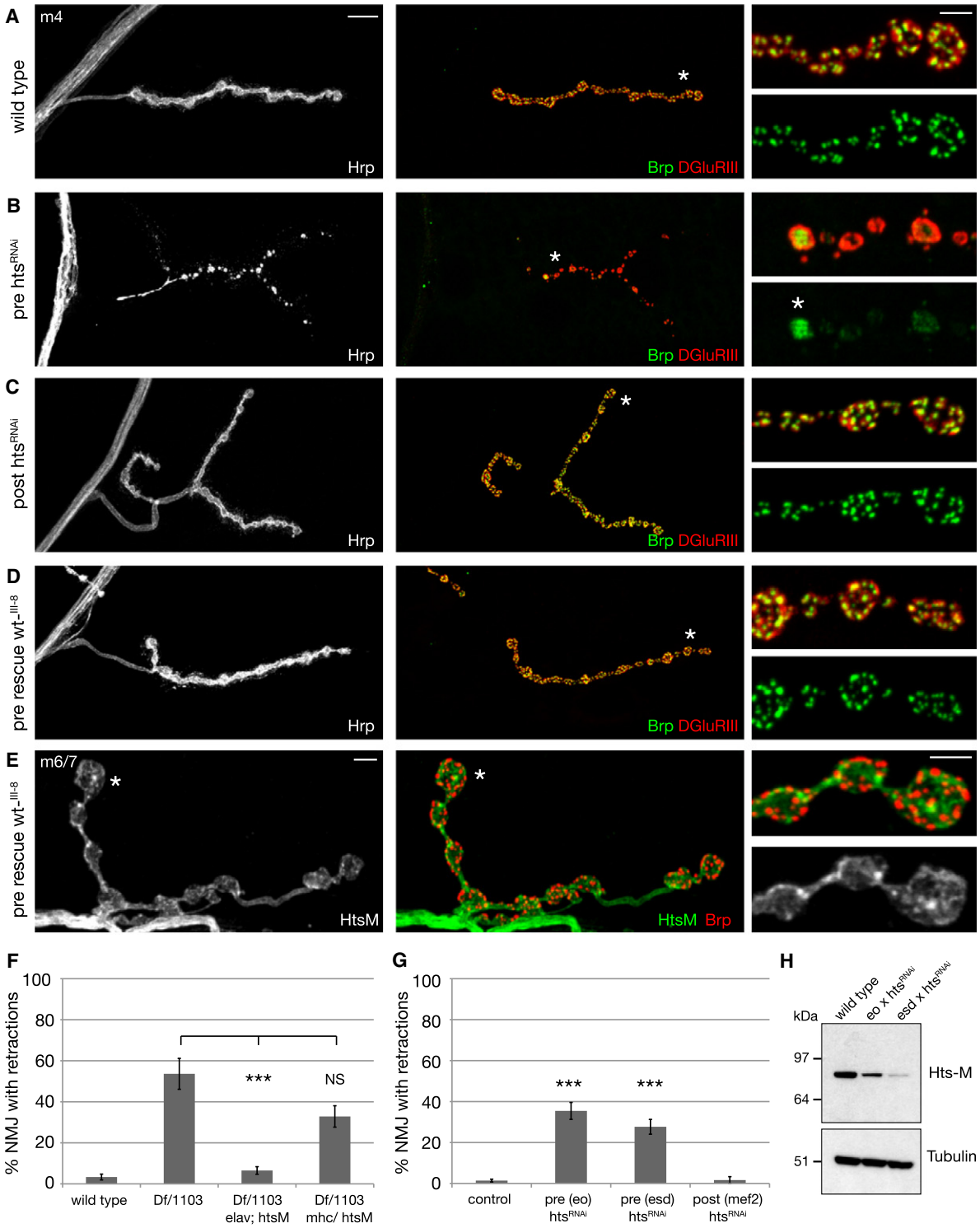

Figure 4. Presynaptic Hts-M Is Both Necessary and Sufficient to Control Synapse Stability

(A–E) Muscle 4 NMJs stained for the presynaptic membrane (HRP, white), presynaptic active zones (Brp, green), and postsynaptic glutamate receptors (DGluRIII, red). (A) Wild-type NMJ showing perfect apposition between pre- and postsynaptic markers. (B) Presynaptic knockdown of *hts* through the expression of a transgenic UAS-*hts*^{RNAi} line by a combination of presynaptic Gal4 lines results in severe presynaptic retractions. In some areas, remnants of Brp remain; however, these are no longer organized into distinct puncta but are uniformly distributed within the altered bouton (asterisk, inset). (C) Postsynaptic knockdown of *hts* in muscle using *mef2*-Gal4. No defects in synapse stability can be observed. (D) Expression of Hts-M in the presynaptic motoneuron using elav-Gal4 in *hts* mutant animals (*elavGal4; Df*^{BSC26}*/hts*^{1103}*; UAS hts-wt*$^{-III-8}$/+) rescues all synapse stability defects associated with the *hts* mutation. Scale bar in (A) applies to (A)–(D) and

Loss of Presynaptic Hts/Adducin Promotes Filopodia-Based NMJ Extension and Synaptogenesis

To this point, the phenotypes caused by loss of *hts/adducin* strongly resemble the effects observed following loss of presynaptic α-/β-Spectrin (Pielage et al., 2005) or presynaptic Ankyrin2L (Pielage et al., 2008). This is consistent with prior demonstration that Adducin is a component of the submembranous spectrin-Ankyrin lattice (Bennett and Baines, 2001). We now describe a phenotype of NMJ expansion that is completely unique to the loss of *hts/adducin*.

The loss of Hts causes two striking phenotypes of enhanced synaptic growth. First, the number of type Ib synaptic boutons is increased by approximately 50% in *hts* mutant animals compared to wild-type controls. This increase in bouton number is observed in all of our mutations and is even stronger (192% compared to control) following RNAi-mediated presynaptic knockdown of Hts (Figures 5B–5H). Furthermore, this phenotype is completely rescued by presynaptic expression of *Hts-M* in *hts* mutant animals ("pre rescue" in Figure 5G). The increase in total bouton number is particularly remarkable given that many of the NMJs that we quantified are also undergoing significant synapse retraction (see above). This aspect is reflected in the large variance of bouton number that we observe in both *hts* mutant and hts^{RNAi} animals (see histogram, Figure 5H). Thus, the quantification of bouton number most likely underestimates the growth-promoting effect caused by loss of presynaptic Hts/Adducin. Based on these data, we conclude that Hts/Adducin also has a potent activity that restricts the expansion and elaboration of the presynaptic nerve terminal.

A second remarkable feature of *hts* mutant NMJs is the appearance of abundant, small-caliber membrane protrusions from the NMJ. These membrane protrusions retain presynaptic proteins like Synapsin and Brp and postsynaptic glutamate receptors, indicating that they may contain functional active zones (Figures 5B, 5C, 5D, and 5F). In many cases, we observe small glutamate receptor clusters at the distal ends of these protrusions that are not yet opposed by presynaptic Brp. This suggests that these are newly forming synapses as live imaging studies previously demonstrated the appearance of postsynaptic glutamate receptors prior to the appearance of the presynaptic active zone marker Brp (Rasse et al., 2005).

Different motoneurons elaborate terminals of different caliber at the *Drosophila* NMJ. The type Ib boutons are large-diameter boutons. The type Is boutons often coinnervate muscles with type Ib. The type II and type III boutons are much smaller caliber boutons and express peptide neurotransmitters. The small-caliber protrusions that we observed originate from existing type Ib boutons, demonstrating that these protrusions represent altered growth of type Ib processes. These small-caliber protrusions are longer and smaller in diameter than "satellite boutons" that have been observed previously in mutations that disrupt synaptic vesicle endocytosis or actin regulators (Coyle et al., 2004; Koh et al., 2004; Marie et al., 2004). Thus, these small-caliber protrusions represent a distinct modification of normal synaptic growth. To quantify this effect, we counted the number of NMJs that contain small-caliber protrusions that emerge from existing type Ib terminals and the average number of protrusions per NMJ. The number of synaptic protrusions is significantly increased in all of the *hts* mutations and after presynaptic knockdown of *hts*, and the severity of this phenotype correlates well with the severity of the allelic combination tested (Figure 5I). These protrusions might directly contribute to the altered growth in *hts* mutant animals because we observe a significant, more than two-fold increase in the number of branches of type Ib terminals on muscle 4 compared to wild-type animals (Figure 5J). Importantly, we can rescue all aspects of altered synapse morphology, protrusions, and branching by presynaptic expression of Hts-M in *hts* mutant animals (Figures 5I and 5J).

Synaptic Protrusions Are Actin-Rich Structures

The phenotype of synaptic overgrowth observed in *hts* mutations is not observed in animals lacking presynaptic α-/β-Spectrin or Ankyrin2L, suggesting that this phenotype may be derived from a unique activity of Hts/Adducin. Prior work in other systems has demonstrated that Adducin is an actin-capping protein that caps the barbed end of actin filaments (Kuhlman et al., 1996; Li et al., 1998). The appearance of small-caliber membrane protrusions would correlate well with a loss of actin capping activity within the presynaptic nerve terminal. We tested the potential actin-capping activity of Hts-M by monitoring the decay in fluorescence of pyrene-labeled actin filaments in the presence of latrunculinB. The addition of purified Hts-M significantly prevents the depolymerization of actin filaments to a similar extent as Capping Protein. The depolymerization rate drops from 11.7 to 1.2 a.u./s (n = 3) (Figures 6A and 6B). This demonstrates that *Drosophila* Hts-M, similar to vertebrate Adducin, has significant actin capping activity. Therefore, we hypothesize that synaptic overgrowth and the appearance of small-caliber synaptic protrusions may be related to the loss of actin-capping activity normally provided by presynaptic Hts-M.

represents 10 μm. Scale bar in insets represents 2 μm. (E) In the rescued animals (pre-rescue *hts*, genotype as in D) we can visualize the localization of presynaptic Hts protein due to the absence of muscle Hts protein. Muscle 6/7 NMJ stained for Hts-M (green), the presynaptic active zone protein Brp (red) and the presynaptic membrane (HRP, white). Scale bar 5 μm, inset 2 μm.

(F) Quantification of synapse retractions in *hts* mutant and rescued animals. Presynaptic expression of Hts-M in *hts* mutant animals (*elavGal4; Df^{BSC26}/hts^{1103}; UAS hts-wt^{III-8}*/+) significantly rescues the synapse retraction phenotype ($p > 0.001$, ANOVA). Postsynaptic expression of Hts-M in *hts* mutant animals (*Df^{BSC26}/hts^{1103}; UAS hts-wt^{III-8}/mhcGal4*) does not significantly rescue the retraction phenotype. The morphology of the NMJ is severely altered in these animals (see Figure S4). (n = number of NMJs: WT = 120, *Df^{BSC26}/hts^{1103}* = 107, *Df^{BSC26}/hts^{1103}*; *elav/* Hts-M = 230, *Df^{BSC26}/hts^{1103}*; *mhc/* Hts-M = 62).

(G) Quantification of synapse retractions after pre- or postsynaptic knockdown of Hts. Abbreviations: control = Gal4 × w^{1118}; pre (eo) = *elavGal4*; *ok371Gal4*; pre (esd) = *elavGal2*; *scaGal4* UAS-*dcr2*; post (*mef2*) = *mef2Gal4* (n = number of NMJs: control = 280, pre (eo) hts^{RNAi} = 98, pre (esd) hts^{RNAi} = 110, post (*mef2*) hts^{RNAi} = 60; *** indicates $p < 0.001$, ANOVA). Error bars represent SEM.

(H) Western blot of Hts protein levels in third-instar larval brains of wild-type and after presynaptic hts^{RNAi} expression.

See also Figures S4 and S5.

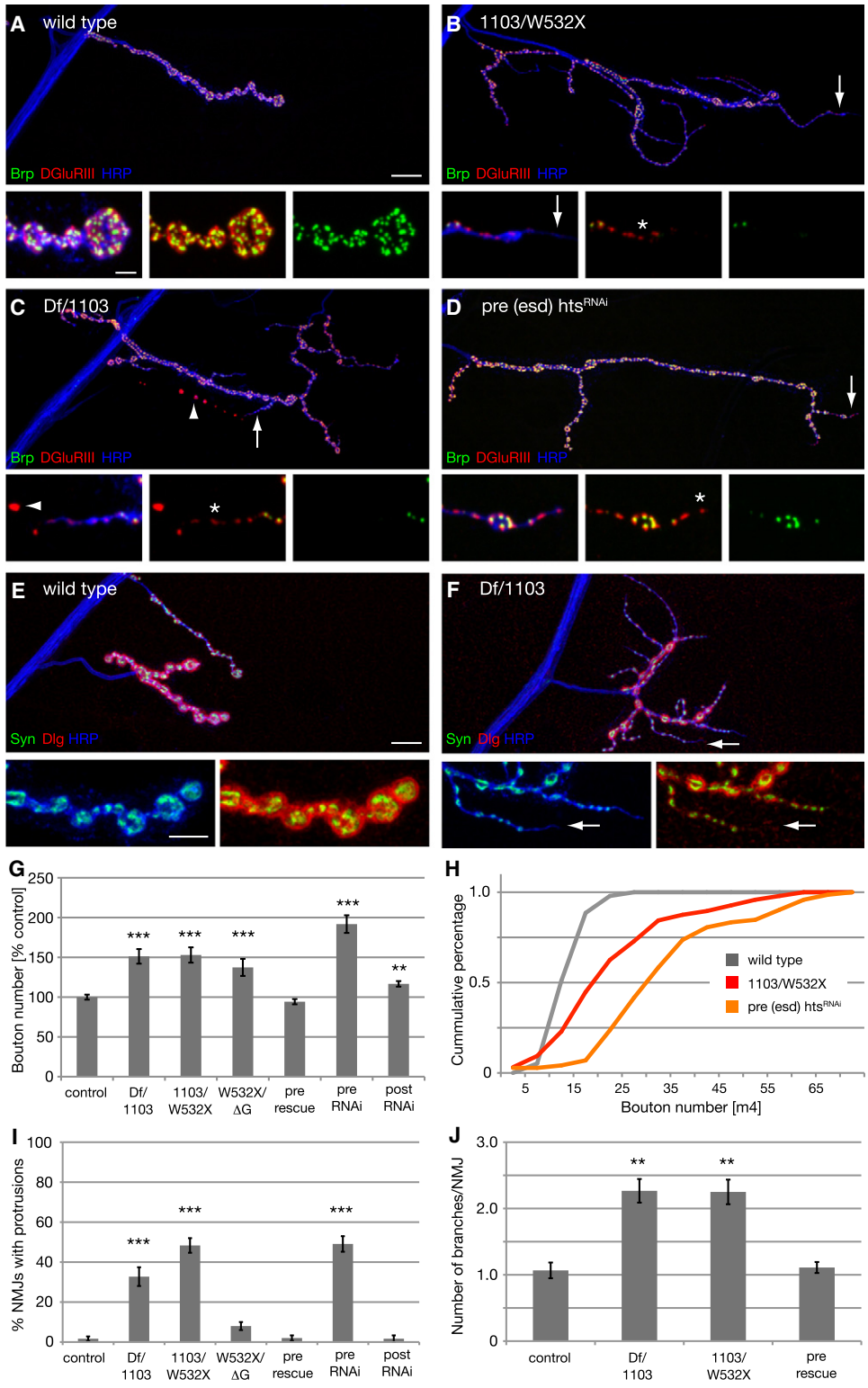

Figure 5. Loss of Presynaptic *hts* Leads to Increased NMJ Growth

(A–D) Muscle 4 NMJs stained for presynaptic active zones (Brp, green), postsynaptic glutamate receptors (DGluRIII, red) and the presynaptic membrane (HRP, blue). (A) Wild-type NMJ. Insets show the precise apposition between pre- and postsynaptic markers. (B) An hts^{1103}/hts^{W532X} mutant NMJ. Mutant animals show a significant increase in NMJ span and bouton number. Aberrant formation of new synaptic boutons can be observed. Long membrane protrusions form with a smaller diameter than normal type Ib boutons. At the ends of these protrusions (arrow, insets), the appearance of small glutamate receptors can be observed

Recently, actin-capping proteins have been hypothesized to regulate a balance between actin-based filopodial extension and the formation of lamellipodial actin networks by Arp2/3-mediated branching (Akin and Mullins, 2008; Bear et al., 2002; Iwasa and Mullins, 2007; Mejillano et al., 2004; van der Gucht et al., 2005). Monomeric actin has a higher affinity for the barbed end of elongating actin filaments than for Arp2/3, and increasing the concentration of capping protein in vitro inhibits filament elongation to promote lamellipod formation by Arp2/3 (Akin and Mullins, 2008). Thus, loss of an actin-capping protein might be expected to bias a cell toward actin filament extension. Consistent with this hypothesis, depletion of capping protein results in a dramatic increase of actin-rich filopodia in tissue culture (Mejillano et al., 2004). Similarly, loss of Eps8, a protein with actin-capping activity, causes the appearance of actin-rich filopodia in cultured neurons (Menna et al., 2009). Based upon these prior studies, we hypothesize that loss of Hts-M/Adducin-mediated actin capping causes actin-based filopodia extensions at the nerve terminal. If so, the small-caliber protrusions that we observe at the NMJ should be actin-rich structures.

We examined filamentous actin within the presynaptic nerve terminal of wild-type and *hts* mutant animals by expression of the f-actin binding domain of *Drosophila* Moesin (UAS-GMA) (Dutta et al., 2002). Consistent with prior studies examining actin at the *Drosophila* NMJ (Nunes et al., 2006), actin is organized into a network near the plasma membrane, including the presence of actin patches that are distributed throughout the NMJ (Figure 6C). In *hts* mutants, we find that the small-caliber nerve terminal protrusions that are opposed by small postsynaptic glutamate receptor clusters are actin rich structures, resembling actin-based filopodia extensions in other systems (Figure 6D, insets).

We next asked whether the small-caliber protrusions also contain bundled microtubules. In wild-type animals, the microtubule-associated protein Futsch labels a core of bundled microtubules that extend throughout the NMJ including all distal boutons (Figures 6E and S6C; Roos et al., 2000). Futsch-positive microtubules do not invade the small-caliber, actin-based protrusions we observed in the *hts* mutants (Figures 6F and S6D, insets). We then analyzed the distribution of the spectrin adaptor protein Ank2L. In wild-type NMJ, Ank2L is present beneath the plasma membrane and provides a potential link among cell adhesion molecules, the spectrin skeleton, and presynaptic microtubules (Figures S6A and S6C; Koch et al., 2008; Pielage et al., 2008). Similar to Futsch, Ank2L is not present in the distal parts of the actin-rich protrusions (Figures S6B and S6D, inset). Finally, we stained the small-caliber protrusions in *hts* mutants for the cell-adhesion molecule Fasciclin II (FasII). FasII is essential for the maintenance of the NMJ as a *trans*-synaptic homophilic cell-adhesion molecule and normally delineates the NMJ (Schuster et al.; Figure S6E). We find that FasII is present in the small-caliber protrusions, indicating that these structures may be stabilized by homophilic cell adhesion (Figure S6F). However, postsynaptic Dlg levels are low, providing additional evidence that these structures may be newly formed, prior to the elaboration of the postsynaptic SSR (Figure S6F). Based upon these data, we propose that the small-caliber protrusions observed in *hts* mutants are derived from increased actin-filament formation caused by the lack of Hts-M-dependent actin capping. Note, however, that in the $hts^{\Delta G}$ mutation lacking the MARCKS domain, we do not observe significant protrusions but we do observe increased growth. It is possible that some actin-capping activity is retained in this mutant based upon prior in vitro biochemistry on vertebrate Adducin proteins (Li et al., 1998) and this is sufficient to suppress protrusion formation (see also Discussion).

Hts/Adducin Overexpression Blocks Extension of Small-Caliber Presynaptic Terminals

If loss of the actin-capping activity of Hts promotes the formation of actin-based filopodial extensions from an existing nerve terminal, then overexpression of Hts-M should block this process. We overexpressed high levels of Hts-M presynaptically and examined synapse morphology at muscles 12 and 13. These muscles are innervated by motoneurons that form large diameter type Ib boutons as well as small caliber type II and type III nerve terminals (Figure 7A). Overexpression of *Hts-M* severely impacts the extension and growth of the small-caliber type II and type III synaptic bouton arborizations (Figure 7B). The motoneurons navigate to the NMJ but fail to extend on the muscle surface. In addition, the morphology of the remaining type III terminals is clearly altered (Figure 7B, arrows). By contrast, the large-caliber type Ib boutons are present and elaborate at the nerve terminal. The quantification of the total length of type III terminals on muscle 12 reveals a significant, 2.7-fold reduction (Figures 7C and 7D). These data support the hypothesis that the actin-capping activity of Hts/Adducin may control the shape and

that are not yet opposed by presynaptic Brp (asterisk). (C) A Df^{BSC26}/hts^{1103} mutant NMJ. On the same muscle, a retracting branch and an overgrown NMJ can be observed. The retraction can be clearly identified through the absence of Brp and the simultaneous fragmentation of the presynaptic membrane (arrowhead). In contrast, new synapses form along continuous protrusions of the presynaptic membrane (asterisk). (D) Presynaptic knockdown of *hts* results in an identical phenotype. Scale bar in (A) applies to (A)–(D) and represents 10 μm, scale bar in inset represents 2 μm.

(E and F) Muscle 4 NMJs stained for the presynaptic vesicle marker Synapsin (green), the postsynaptic SSR marker Dlg (red), and the presynaptic membrane (HRP, blue). Insets show distal part of the NMJ at higher magnification. Scale bar in (E) applies to (E) and (F) and represents 10 μm; scale bar in inset 5 μm.

(G) Quantification of boutons numbers. Numbers are normalized to control genotypes. The NMJ overgrowth can be completely rescued through presynaptic expression of Hts-M in Df^{BSC26}/hts^{1103} mutant animals (pre-rescue). There is no difference in muscle size between genotypes. (n = NMJs per genotype: control = 96, hts^{1103}/Df^{BSC26} = 96, hts^{1103}/hts^{W532X} = 96, $hts^{W532X}/hts^{\Delta G}$ = 40, pre-rescue = 96, pre-RNAi = 72, post-RNAi = 64; *** indicates $p < 0.001$, ** indicates $p < 0.01$ compared to control, ANOVA).

(H) Histogram of bouton numbers for selected genotypes from (G).

(I) Quantification of protrusions. Protrusions were quantified as HRP positive protrusions that show glutamate receptors with little or no opposing Brp staining (n = NMJs per genotype: control = 120, hts^{1103}/Df^{BSC26} = 107, hts^{1103}/hts^{W532X} = 120, $hts^{W532X}/hts^{\Delta G}$ = 100, pre-rescue = 98, pre-RNAi = 110, post-RNAi = 60; *** indicates $p < 0.001$ compared to control, ANOVA).

(J) Quantification of the number of branches per NMJ (** indicates $p < 0.01$, ANOVA). Numbers as in (I). Error bars represent SEM.

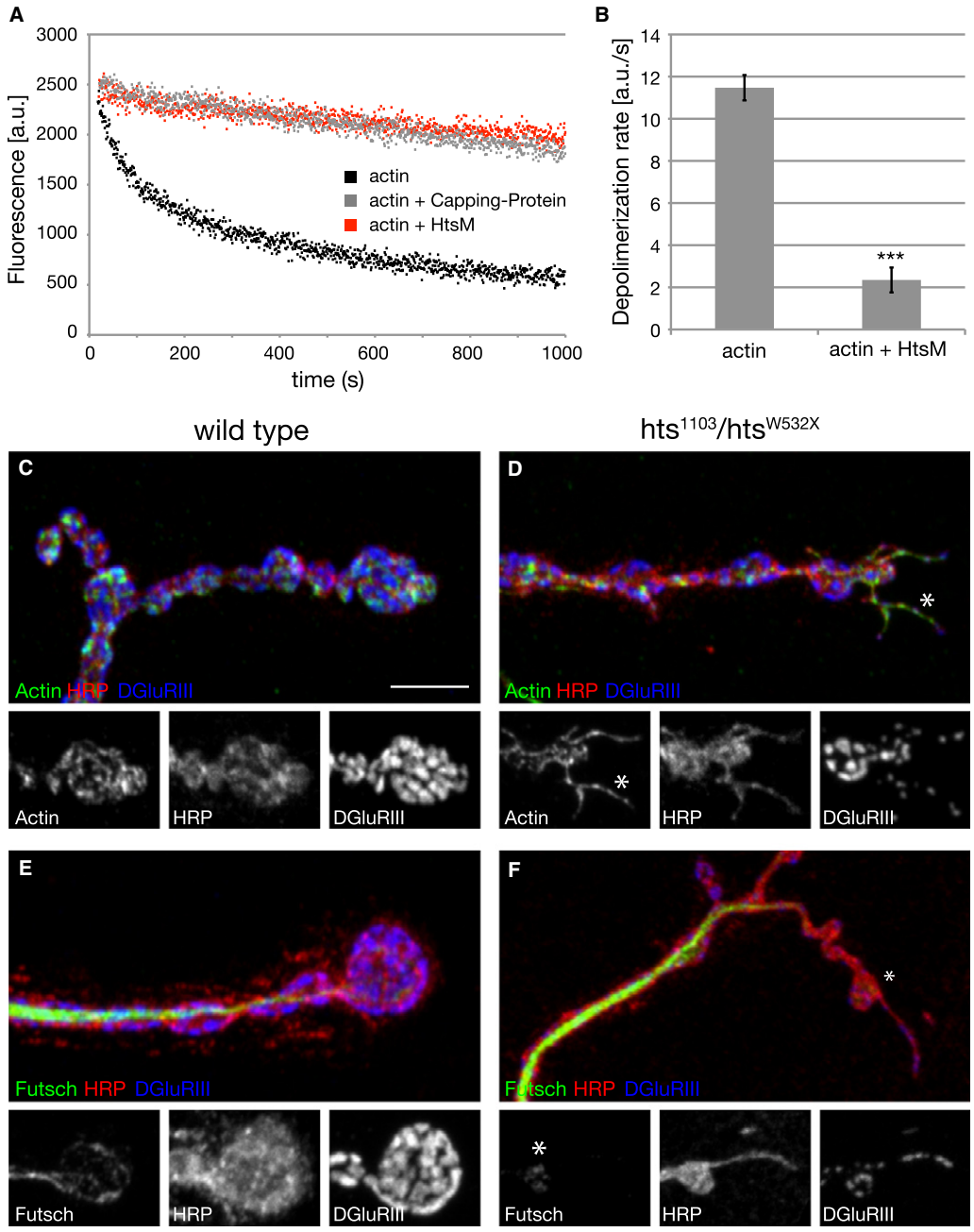

Figure 6. *Drosophila* Hts-M Is an Actin-Capping Molecule

(A) Pyrene-labeled actin filaments were diluted to 500 nM into KMEI plus 1 μM latrunculin B to stimulate depolymerization. The assay was performed alone (black) or in the presence of Hts-M (red) or capping protein (gray). Hts-M protects actin filaments from depolymerization to a similar extent as capping protein.

(B) Rate of depolymerization of actin filaments from (A), calculated from the initial 60 s of the reactions (three independent trials per assay). The presence of Hts-M in the assay reduces the depolymerization rate from 11.696 to 1.221 a.u./s; *** indicates $p < 0.001$, Student's t test; error bars represent SEM.

(C) Presynaptic actin filaments were visualized through the expression of the GFP-tagged f-actin binding domain of *Drosophila* Moesin (UAS-GMA).

(D) In the absence of Hts-M, membrane protrusions are evident at many sites of the presynaptic nerve terminal. Actin filaments are present throughout the protrusions (asterisk, insets).

(E) In wild-type, microtubules are present and form loops in distal synaptic boutons (anti-Futsch).

(F) In *hts* mutant animals, Futsch staining is absent in the distal parts of the protrusions.

Scale bar in (C) corresponds to (C)–(F), 5 μm. See also Figure S6.

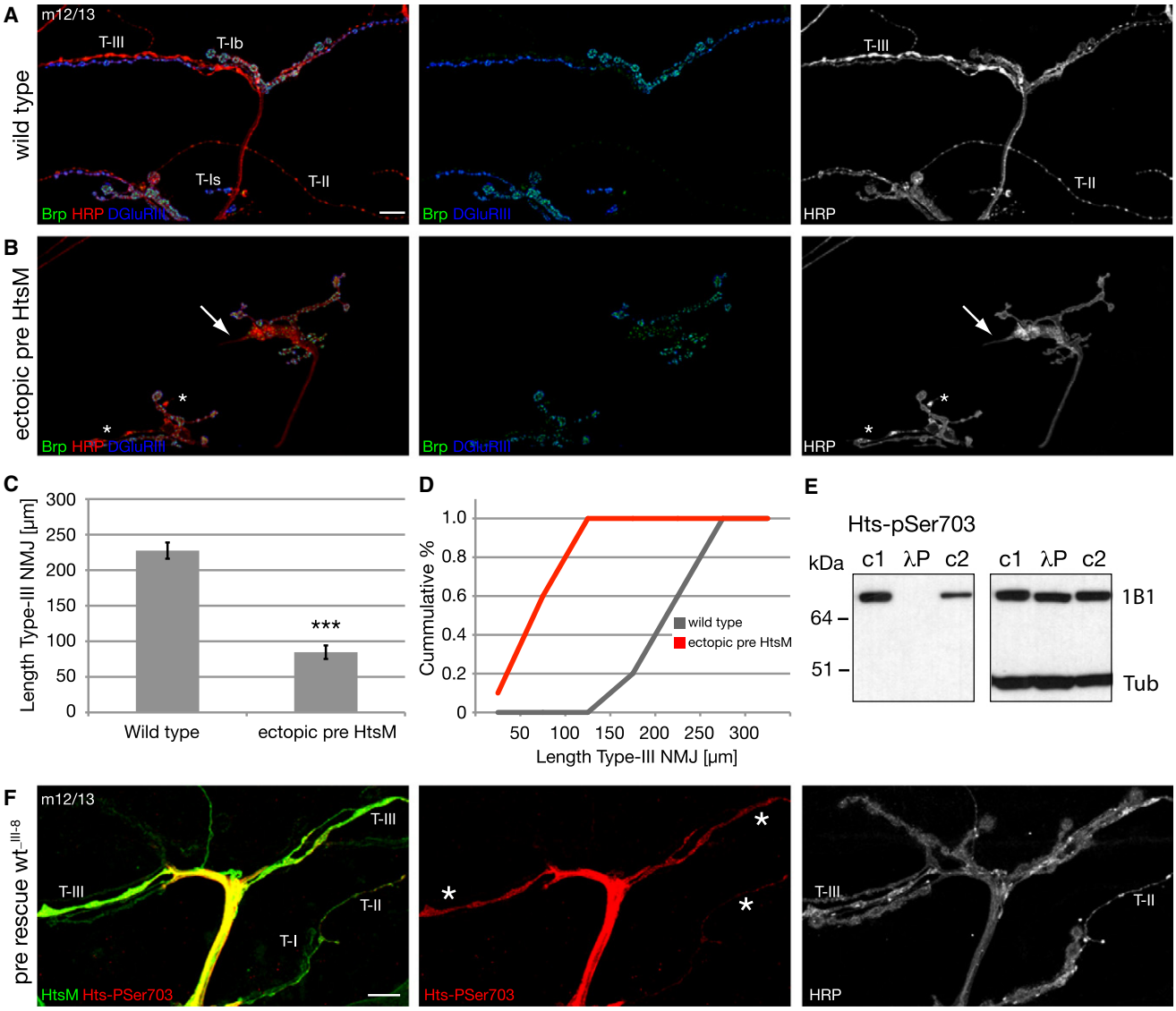

Figure 7. Ectopic Expression of Hts-M Can Restrict Synapse Formation and Growth

(A–C) NMJs on muscles 12/13 stained for the presynaptic active zone protein Brp (green), the presynaptic membrane (HRP, red), and postsynaptic glutamate receptors (DGluRIII). (A) Wild-type NMJ. Type II and III synapses cover large areas of muscles 12 and 13. (B) Expression of high levels of Hts-M presynaptically in a wild-type background (*elav*Gal4; *sca*Gal4 crossed to two copies of UAS-Hts-M). Synapse formation of type II and type III synapses is severely suppressed. The arrows indicate the tip of type III synapses with altered morphology, and the asterisks indicate type II synapses. (C and D) Quantification of NMJ length of type III synapses. The ectopic expression of Hts-M reduces the mean total length of type III synapses on muscle 12 from 227 µm to 84 µm ($n = 10$); $p < 0.001$ compared to wild-type, ANOVA; error bars represent SEM).

(E) The Hts-pSer703 (UPS) antibody recognizes only phosphorylated Hts-M. In untreated larval brain extracts (c1 and c2) anti-Hts-pSer703 detects a protein of identical size as the Hts-1B1 antibody (right blot). The signal is absent in larval brain extracts treated for 30 min with λ-phosphatase (λP). c1: identical buffer as in λP treated lane including phosphatase inhibitors; c2: standard Ripa buffer including phosphatase inhibitors. The image on the right is the same western blot after stripping analyzed with anti-Hts-1B1 and anti-Tubulin antibody.

(F) To analyze the distribution and phosphorylation level of presynaptic Hts-M we stained *hts* mutant animals that expressed Hts-M only presynaptically (*elavGal4; Df*^{BSC26}*/hts*^{1103}*; UAS hts-wt*$^{-III-8}$/+). In these animals, all phenotypes associated with *hts* mutations are rescued. We analyzed the distribution of the Hts-M and phospho-Hts at muscles 12/13, where we can simultaneously analyze type I, II, and III synapses as stated in (A). While we detect no or only very low levels of phosphorylated Hts-M in type I boutons, we observe high levels of phosphorylated Hts-M in both type II and type III synapses.

Scale bar in (A) corresponds to (A), (B), and (F), 10 µm. See also Figure S7.

extent of nerve terminal growth, particularly of the small-caliber synaptic arborizations. Interestingly, the small-caliber nerve terminals (type II and type III) are the most dynamic structures in the neuromuscular system and are strongly influenced by changes in neural activity (Budnik et al., 1990). This raises the possibility that Hts activity might be regulated to control synaptic growth.

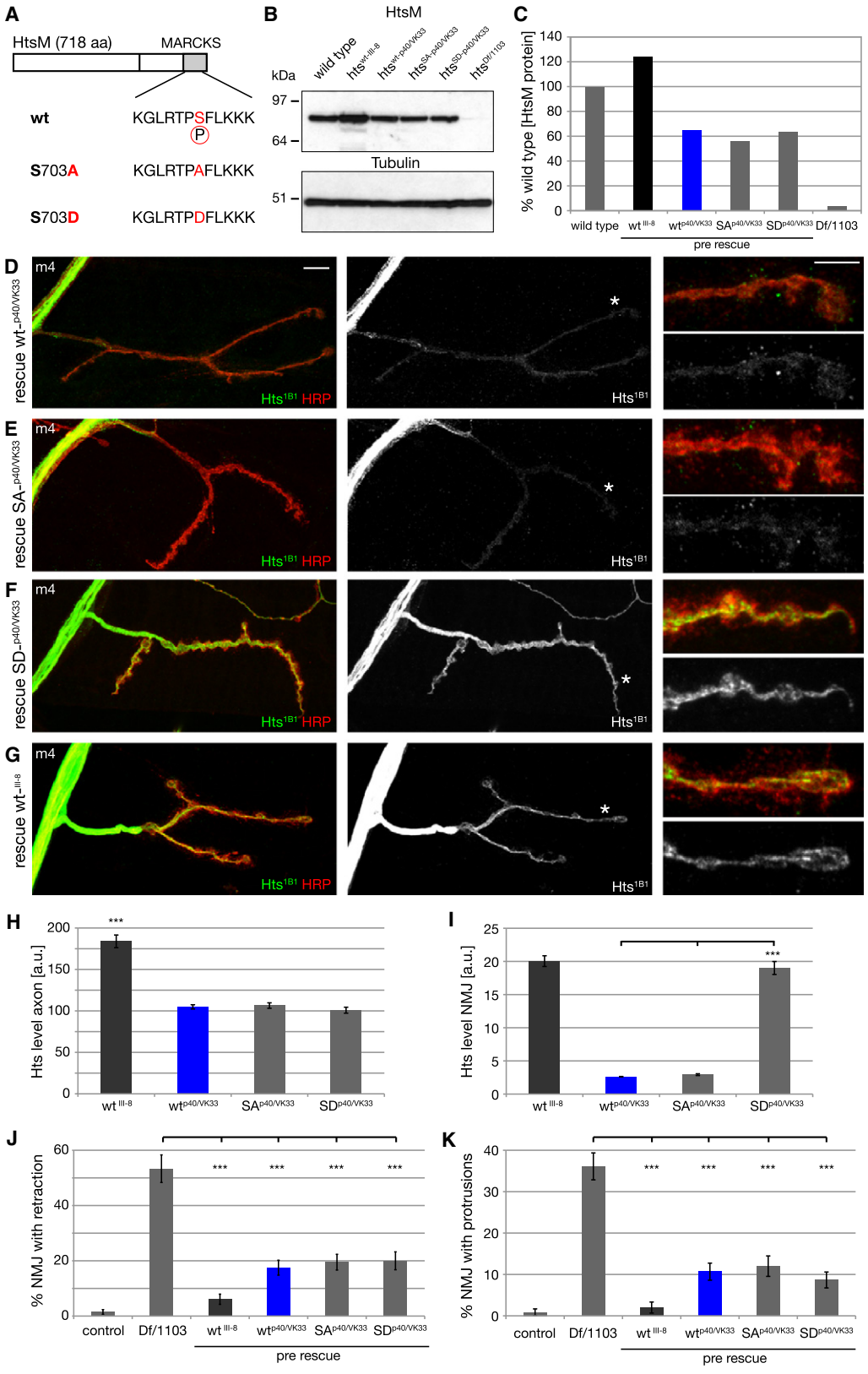
A
HtsM (718 aa)
MARCKS
wt
KGLRTPSFLKKK
P
S703A
KGLRTPAFLKKK
S703D
KGLRTPDFLKKK
B
HtsM
kDa
wild type
htsIII-8
htswt-p40/VK33
htsSA-p40/VK33
htsSD-p40/VK33
htsDf/1103
97
64
Tubulin
51
C
% wild type [HtsM protein]
wild type
wt III-8
wtp40/VK33
SAp40/VK33
SDp40/VK33
Df/1103
pre rescue
D
rescue wt-p40/VK33
m4
Hts1B1 HRP
Hts1B1
E
rescue SA-p40/VK33
F
rescue SD-p40/VK33
G
rescue wt-III-8
H
Hts level axon [a.u.]
I
Hts level NMJ [a.u.]
J
% NMJ with retraction
control
Df/1103
K
% NMJ with protrusions

Evidence for Phosphorylation-Dependent Control of Synaptic Hts/Adducin

The spectrin-binding and actin-recruiting functions of Adducin, as well as its subcellular localization, are controlled by phosphorylation in several tissues in vertebrates. For example, in resting platelets, dephosphorylated Adducin is complexed with the submembranous spectrin skeleton where it may cap actin filaments and inhibit filopodia formation. During platelet activation, Adducin becomes phosphorylated, released from the submembranous spectrin skeleton, and aggregates in the cell interior. It is believed that the translocation of Adducin removes actin-capping activity from the membrane and enables the observed change in platelet cell shape that includes the formation of numerous filopodia (Barkalow et al., 2003). By extension, we might expect to observe phosphorylated Hts/Adducin at synapses undergoing actin-based extension and growth. We tested this possibility using available phosphospecific antibodies. The anti-phospho-Adducin (Ser724) antibody (Upstate/Millipore) was raised against a peptide corresponding to amino acids 720–728 of rat α-Adducin. This peptide FRTP[pS]FLKK is, except for the first amino acid, identical to the core sequence of the MARCKS domain of *Drosophila* Hts-M (see Figure 1A). We refer to this antibody as Hts-pSer703 based on the position of the phosphorylated Serine in the *Drosophila* Hts-M sequence.

First, we demonstrate that Hts-pSer703 is indeed a phospho-specific Hts antibody that works in situ at the *Drosophila* NMJ (Figures S7A and S7B). Hts-pSer703 staining is observed both in the presynaptic motor nerve and throughout the muscle (Figure S7A), where it colocalizes with Hts-M. Importantly, all staining is absent in *hts* mutant animals indicating specificity for *Drosophila* Hts-M (Figure S7B). To demonstrate that Hts-pSer703 only recognizes phosphorylated Hts-M, we analyzed larval brain extracts in the presence or absence of λ-phosphatase. The λ-phosphatase treatment completely abolishes any signal on the western blot (Figure 7E). In addition, a small downshift of the Hts-M protein can be detected when analyzing the extract with a general Hts antibody, suggesting several phosphorylations of Hts-M in vivo (Figure 7E, right blot Hts1B1). Therefore, we can conclude that a subset of Hts-M is phosphorylated both in the presynaptic nerve and in postsynaptic muscle.

In order to determine whether phosphorylated Hts-M is present within the presynaptic nerve terminal, we used our presynaptic rescue assay that allows the visualization of presynaptic Hts-M protein in absence of postsynaptic Hts-M protein. We first examined type II and III terminals on muscle 12/13 that are most sensitive to Hts-M overexpression (see above; Figures 7B–7D). We observe Hts-M and Hts-pSer703 staining throughout the terminal of both type II and type III boutons (Figure 7F). Interestingly, while Hts-M is clearly present in type Is and Ib terminals on the same muscles, we do not observe significant levels of Hts-pSer703 staining in these boutons. Similarly, if we analyze Hts-M and Hts-pSer703 in type Ib boutons on muscle 4, we find that Hts-pSer703 staining is restricted to the motor nerve and stops just prior to where the motoneuron contacts the muscle cell. There is no or only very low levels of phosphorylated Hts-M protein in the presynaptic terminal of type Ib boutons, although there is clearly abundant Hts-M protein within the presynaptic nerve terminal (Figure S7C). We conclude that Hts-M is dephosphorylated within type Ib boutons. We hypothesize, therefore, that Hts-M may be regulated by posttranslational phosphorylation within small-caliber type II and type III terminals, and possibly maintained in a dephosphorylated state in type Ib boutons. This differential regulation may account for the enhanced dynamics and plasticity of type II and III nerve terminals compared to the larger caliber type Ib terminals.

We next tested the hypothesis that the phosphorylation status of Hts-M might control the localization of the Hts protein and the function of Hts during NMJ growth and stabilization. Therefore, we generated *hts-M* transgenes harboring either phosphomimic (S703D) or nonphosphorylatable (S703A) mutations within the Hts-M MARCKS domain (Figure 8A). It was necessary to precisely control transgene expression levels in order to compare synaptic protein levels between

Figure 8. Control of Synaptic Hts-M Localization via Phosphorylation of S703

(A) Schematic of the wild-type, nonphosphorylatable (S703A), and phosphomimic (S703D) Hts-M sequences.

(B) Western blot of third-instar larval brains comparing Hts-M levels in wild-type, mutant, and the different presynaptic rescue animals.

(C) Quantification of the western blots. We observe identical expression levels between the site-integrated constructs wt-p40/VK33, SA-p40/VK33, and SD-p40/VK33 in the mutant background. The P-element-mediated insertion wt_III-8 expresses approximately 2-fold higher levels of Hts-M compared to the site-integrated constructs and approximately 120% of wild-type. The site-integrated insertions express only approximately 60% of wild-type Hts-M levels.

(D–G) Visualization of axonal and presynaptic Hts-M levels in rescued animals expressing different Hts-M constructs presynaptically (genotypes as in B and C) on muscle 4. The site-integrated constructs (D–F) express identical levels of WT, SA, and SD mutant forms of Hts-M. Animals are stained with Hts-1B1 and Hrp to mark the presynaptic membrane. (D) Expression of wild-type Hts-M results in very low levels of Hts-M within the presynaptic nerve terminal. (E) Expression of nonphosphorylatable Hts-M (SA) results in similarly low levels of Hts-M within the presynaptic nerve terminal. (F) Expression of a phosphomimic form of Hts-M (SD) results in highly abundant Hts-M protein within the presynaptic nerve terminal. (G) The P element insertion wt_III-8 used for all phenotypic rescues (Figure 4) expresses high levels of Hts-M in the presynaptic nerve terminal.

(H) Quantification of Hts-M levels in the axon. Identical levels can be observed for the three site-integrated constructs while the P element insertion shows an approximate 2-fold increase, corresponding to the 2-fold higher expression levels observed in (B) and (C).

(I) Quantification of Hts-M levels within the presynaptic nerve terminal. The presynaptic levels of the Hts-SD variant are approximately 5-fold increased compared to WT and SA variants.

(J) Quantification of synapse retractions at m4 for the different phenotypes.

(K) Quantification of protrusions on m4. All constructs significantly rescue the protrusion phenotype. The original wild-type construct that expresses higher levels of Hts rescues better than the site-integrated versions ($n > 150$ for all genotypes for J and K; *** indicates $p < 0.001$, ANOVA; error bars represent SEM).

See also Figure S8.

phosphomimic and nonphosphorylatable transgenes. To address this, we took advantage of the recently developed phi-mediated site-specific integration system in *Drosophila* (Venken and Bellen, 2007). We generated transgenic lines with transgenes inserted at specific genomic integration sites for wild-type (WT), phosphomimic (SD), and nonphosphorylatable (SA) forms of Hts-M. We had to generate stocks that allow presynaptic expression of two UAS-insertions (attP40 and VK00033 insertions of the same transgenes) in the background of the *hts* mutation to achieve significant expression levels in motoneurons (see Experimental Procedures). First, we assayed expression levels of Hts-M protein in the larval brains of these rescued animals (e.g., for wild-type: $hts^{wt\text{-}p40/VK33}$ = elavGal4; hts^{1103} UAS-*hts-M-*wt^{p40}/Df(2R)BSC26; UAS-*hts-M-*wt^{VK33}). We find equivalent protein expression levels for each genotype assayed by western blot (Figures 8B and 8C). Each of these site integrated Hts-M variants is expressed at approximately 60% of wild-type Hts-M levels (Figures 8B and 8C). By comparison, the wild-type Hts-M transgene ($wt^{III\text{-}8}$ = random P element insertion on the third chromosome) that we used in our prior rescue experiments is expressed at approximately 120% of wild-type levels (Figures 8B and 8C). Thus, we have a system that allows us to express wild-type and modified Hts proteins in the *hts* mutant background and make direct comparisons between these genotypes regarding synaptic protein levels and phenotypic rescue.

The first striking observation is that the phosphomimic transgene ($hts^{SD\text{-}p40/VK33}$) results in significantly higher levels of synaptic Hts-M protein compared to either the wild-type ($hts^{wt\text{-}p40/VK33}$) or the nonphosphorylatable transgene ($hts^{SA\text{-}p40/VK33}$) (Figures 8D–8F). This difference in synaptic localization is reproducible and quantifiable (Figure 8I; SD is more than five times more abundant within the presynaptic nerve terminal compared to WT and SA). By contrast, there is no difference in the levels of axonal protein levels among the three transgenes, consistent with equivalent protein expression levels detected in larval brain extracts (Figure 8H). Furthermore, expression of our original wild-type transgene ($wt^{-III\text{-}8}$) shows increased protein levels both in the axon and at the synapse compared to the phi-integrated wild-type transgenes ($hts^{wt\text{-}p40/VK33}$) (Figures 8G–8I). From these data, we conclude that the phosphomimic S703D mutation facilitates trafficking of Hts M protein into the presynaptic nerve terminal, which could include mechanisms of protein transport or stabilization.

We next asked whether the mutant transgenes had a differential ability to rescue the phenotypes of synaptic retraction, bouton number, and the appearance of growth-related protrusions in the *hts* mutant. Both the phosphomimic and nonphosphorylatable transgenes were able to significantly rescue synapse retractions (Figure 8J), protrusions (Figure 8K), and bouton numbers (Figure S7). Thus, the primary effect of the phosphomimic mutation appears to be the control of synaptic translocation of the Hts-M protein. However, if one takes into account the different levels of synaptic protein present in WT, phosphomimic and nonphosphorylatable genotypes, then some phenotypic differences can be observed. For example, comparing $hts^{wt\_III\text{-}8}$ to $hts^{SD\text{-}p40/VK33}$, which show equivalent synaptic Hts-M protein levels, reveals that $hts^{SD\text{-}p40/VK33}$ does not rescue as well (Figures 8J and 8K). This could indicate that the mutant protein is not fully functional or that the phosphorylation-dependent localization of the mutant protein is not optimal. Regardless, the major effect of S703 phosphorylation within the MARCKS domain appears to be to control Hts synaptic protein levels, a parameter that we have shown can strongly influence synapse stability and growth.

DISCUSSION

Here, we provide evidence that Hts/Adducin is an important player in the mechanisms that control both the stability and growth of the NMJ. We demonstrate that *hts* mutations cause a profound destabilization of the presynaptic nerve terminal. These data are consistent with the well-established function of Adducin as a spectrin-binding protein that participates in the stabilization of the submembranous spectrin-actin skeleton (Bennett and Baines, 2001; Matsuoka et al., 2000). Remarkably, *hts* mutations also promote the growth and elaboration of new processes at the NMJ. Indeed, the elaboration of new processes and increased growth overcome the effects of synapse destabilization such that, on average, the NMJ is significantly larger in the *hts* mutant animals compared to wild-type. Process elaboration is accompanied by the extension of small-caliber, actin-rich protrusions that contain the necessary machinery for synaptic transmission including essential components of the active zone, postsynaptic glutamate receptors, and homophilic cell-adhesion molecules. This phenotype has not been observed in animals lacking presynaptic α-/β-Spectrin or Ankyrin2 (Pielage et al., 2005, 2008), indicating that Hts/Adducin has a specific activity relevant to the formation of these new synaptic processes.

We go on to provide biochemical insight into how Hts/Adducin might control new process formation at the NMJ. We demonstrate that *Drosophila* Hts-M has actin-capping activity similar to its vertebrate homolog. Based on recent work in other systems, loss of actin-capping activity at the plasma membrane could reasonably favor the formation of actin-based filopodia that might promote the elaboration of small-caliber synaptic protrusions (Bear et al., 2002; Mejillano et al., 2004; Menna et al., 2009). Consistent with such a model, overexpression of Hts/Adducin, thereby increasing the amount of actin-capping protein at the NMJ, is sufficient to inhibit the growth and elaboration of small-caliber type II and type III nerve terminals. Finally, we demonstrate that synaptic localization of Hts/Adducin is controlled via phosphorylation of a conserved serine residue in the C-terminal MARCKS domain. Based on these and additional data discussed below, we present a model in which Hts/Adducin functions as a molecular keystone, stabilizing the submembranous spectrin skeleton to achieve synapse stability and simultaneously capping actin filaments at the plasma membrane to influence the shape and growth potential of the presynaptic nerve terminal. Modulation of Adducin activity, either through changes in protein abundance or phosphoregulation, might then influence the balance of growth versus stability (see also Bednarek and Caroni, 2011 [this issue of *Neuron*]).

Mechanisms of Remodeling and Degeneration

Synapse retraction at the *Drosophila* NMJ occurs without cell death (Eaton et al., 2002; Massaro et al., 2009) implying a local

degenerative process. Mechanistically, withdrawal of target-derived BMP signaling causes retraction (Eaton and Davis, 2005) while overexpression of BMPs can suppress retractions (Massaro et al., 2009), suggesting similarities with developmental remodeling. However, we have identified several mutations that cause NMJ retraction that are linked to neuromuscular degeneration in human (Eaton et al., 2002; Pielage et al., 2005). Furthermore, overexpression of a Wld^S (Wallarian degeneration slowed) transgene is able to significantly suppress synapse retraction at the NMJ, implying a degenerative mechanism similar to that observed in mammalian motoneurons (Massaro et al., 2009). Based upon these data, we hypothesize that synapse retraction at the *Drosophila* NMJ is driven by local, degenerative processes that are similar to those observed during neural development and the early stages of neurodegeneration in other systems.

Our data demonstrating the involvement of Hts/Adducin in both NMJ degeneration and nerve terminal sprouting/growth is quite unique. It may be possible to partition these functions to the spectrin-binding and actin-capping activities of Adducin. It is particularly intriguing that the subcellular distribution of Adducin can be regulated by phosphorylation. Might changes in the local concentration of Adducin be involved in developmental pruning and neuromuscular synapse elimination or degeneration in other systems? If so, our data seem to highlight an increasingly opaque distinction between degenerative and developmental mechanisms.

Enhanced NMJ Growth, Altered NMJ Morphology, and Regulation of Synaptic Actin

Two general phenotypes of synaptic overgrowth have been previously documented at the *Drosophila* NMJ. The first phenotype involves a uniform and dramatic expansion of the NMJ (DiAntonio et al., 2001; Wan et al., 2000; Sweeney and Davis, 2002). The second phenotype involves the formation of highly ramified clusters of synaptic boutons that have been termed satellite boutons (Marie et al., 2004). This phenotype has been linked to disruption of endocytic proteins such as Dap160/Intersectin, Dynamin, and Endophilin (Koh et al., 2004; Marie et al., 2004) as well as mutations that disrupt actin regulatory molecules including Wasp, Arp2/3, and Nervous Wreck (Coyle et al., 2004).

By contrast, the phenotypes documented in *hts/adducin* are quite different from any previously reported mutation. The NMJ is transformed into a hybrid structure consisting of normal type Ib boutons that support the extension of long, small-diameter synaptic protrusions. This phenotype is robust and highly penetrant. Adducin has two prominent functions. It participates in the stabilization of the spectrin-ankyrin skeleton and it caps actin filaments. By comparison of our data with prior genetic analyses of *α-/β-spectrin* and *ankyrin2L* (Koch et al., 2008; Pielage et al., 2005, 2008), we can partition these two functions of *hts/adducin*. α-/β-Spectrin and Ankyrin2L are necessary for NMJ stability but do not influence NMJ growth. Thus, we propose that Adducin is required to stabilize the nerve terminal through a well-established association with the spectrin/ankyrin skeleton. By extension, we propose that the actin-capping activity of Adducin regulates NMJ growth. One possibility is that loss of actin-capping at the nerve terminal membrane promotes filopodia formation and this drives the extension of the observed small-caliber protrusions. However, the loss of actin-capping activity alone may not be sufficient since it occurs in the presence of an impaired spectrin/ankyrin/adducin submembranous skeleton. An alternative possibility is that loss of Adducin causes two simultaneous effects. First, it relieves a constraining influence of the spectrin skeleton (Pielage et al., 2005). Second, in this relaxed context, increased filopodia formation is able to efficiently drive new nerve-terminal extension. Such a model could explain why the $hts^{\Delta G}$ mutation does not have prominent protrusions despite showing increased growth. If the $hts^{\Delta G}$ mutation retains some actin-binding activity, as suggested by in vitro data (Li et al., 1998), and retains some stabilizing activity (Figure 2), then the combined effect might be sufficient to suppress protrusion formation while allowing enhanced synaptic growth. Interestingly, the association of Adducin with the submembranous spectrin skeleton can be controlled via phosphorylation downstream of growth factor signaling in other systems (Fukata et al., 1999; Pariser et al., 2005).

EXPERIMENTAL PROCEDURES

Fly Stocks

Flies were maintained at 25°C on standard fly food. The following strains were used in this study: w^{1118} (as wild-type), hts^{1103}, *Df(2R)BSC26*, $ank2^{518}$, $ank2^{2001}$ *elav*-GAL4, *mef2*-GAL4, and *mhc*-GAL4 (all Bloomington Stock Center), UAS-*drc2*, hts^{RNAi} (lines 103631 and 29102, Vienna *Drosophila* RNAi center), hts^{W532X}, and $hts^{\Delta G}$ (gift of L. Cooley, New Haven, CT).

Generation of hts Constructs, Transgenes, and Protein

See Supplemental Experimental Procedures.

Immunohistochemistry

Primary antibodies were used at the following dilutions: anti-Bruchpilot (nc82) 1:200, anti-Fasciclin II (1D4) 1:50, anti-Synapsin 1:50, anti-Futsch (22C10) 1:500, anti-Hts-1B1 1:50 (all provided by the Developmental Studies Hybridoma Bank, IA), rat anti-Ank2L 1:500 (gift from M. Hortsch), rabbit anti-Dlg 1:5.000 (gift from V. Budnik), rabbit anti-Syt 1:500, mouse anti-phospho-Adducin (Ser274) (= anti p703-Hts-M) (Upstate/Millipore) 1:400, rabbit anti-Hts-M 1:1000 (gift from L. Cooley); anti-DGluRIII was raised by David's Biotechnology (Regensburg, Germany) against the 22 C-terminal amino acids of DGluRIII as previously reported (Marrus et al., 2004), affinity purified, and used at 1:4000. Alexa488/568/647 conjugated secondary antibodies were obtained from Invitrogen and used at 1:1000. Cy3 and Cy5 conjugated anti-HRP were obtained from Jackson Immunoresearch Laboratories and Molecular Probes and used at 1:1000 dilutions for 1–2 hr at room temperature (RT). Larval preparations were mounted in Prolong. Images were captured at room temperature using a Leica SPE confocal microscope with a HCX PLAPO 63× objective (Aperture 1.4). Imaris software (Bitplane) was used to process and analyze images and to quantify phenotypes.

Western Blot

See Supplemental Experimental Procedures.

Electrophysiology

Third-instar larvae were selected and dissected according to previously published techniques (Pielage et al., 2008). Whole-muscle recordings were performed on muscle 6 in abdominal segment A3 using sharp microelectrodes (12–16 MΩ). Recordings were selected for analysis only if resting membrane potentials were more hyperpolarized than –60 mV and if input resistances were greater than 5MΩ. See Supplemental Experimental Procedures for additional detail.

Electron Microscopy

Methods have been previously published (Pielage et al., 2005, 2006). See also Supplemental Experimental Procedures.

Actin-Capping Assay

Actin was purified from *Acanthamoeba castellani* as described (Gordon et al., 1976), labeled with pyrene iodoacetamide as described (Cooper et al., 1983), and stored on ice. Actin depolymerization assays were performed as described, with minor modification (Zuchero et al., 2009). See Supplemental Experimental Procedures for additional detail.

SUPPLEMENTAL INFORMATION

Supplemental Information includes eight figures and Supplemental Experimental Procedures and can be found with this article online at doi:10.1016/j.neuron.2011.02.007.

ACKNOWLEDGMENTS

We would like to thank V. Budnik, M. Hortsch, and L. Cooley for generous gifts of antibodies and fly stocks. This work was supported by the Novartis research foundation (J.P.) and NIH grant (NS047342) (G.W.D.).

Accepted: January 3, 2011
Published: March 23, 2011

REFERENCES

Akin, O., and Mullins, R.D. (2008). Capping protein increases the rate of actin-based motility by promoting filament nucleation by the Arp2/3 complex. Cell *133*, 841–851.

Barkalow, K.L., Italiano, J.E., Jr., Chou, D.E., Matsuoka, Y., Bennett, V., and Hartwig, J.H. (2003). Alpha-adducin dissociates from F-actin and spectrin during platelet activation. J. Cell Biol. *161*, 557–570.

Bear, J.E., Svitkina, T.M., Krause, M., Schafer, D.A., Loureiro, J.J., Strasser, G.A., Maly, I.V., Chaga, O.Y., Cooper, J.A., Borisy, G.G., and Gertler, F.B. (2002). Antagonism between Ena/VASP proteins and actin filament capping regulates fibroblast motility. Cell *109*, 509–521.

Bednarek, E., and Caroni, P. (2011). β-Adducin is required for stable assembly of new synapses and improved memory upon environmental enrichment. Neuron *69*, this issue, 1132–1146.

Bennett, V., and Baines, A.J. (2001). Spectrin and ankyrin-based pathways: Metazoan inventions for integrating cells into tissues. Physiol. Rev. *81*, 1353–1392.

Bennett, V., Gardner, K., and Steiner, J.P. (1988). Brain adducin: a protein kinase C substrate that may mediate site-directed assembly at the spectrin-actin junction. J. Biol. Chem. *263*, 5860–5869.

Budnik, V., Zhong, Y., and Wu, C.F. (1990). Morphological plasticity of motor axons in Drosophila mutants with altered excitability. J. Neurosci. *10*, 3754–3768.

Budnik, V., Koh, Y.H., Guan, B., Hartmann, B., Hough, C., Woods, D., and Gorczyca, M. (1996). Regulation of synapse structure and function by the *Drosophila* tumor suppressor gene dlg. Neuron *17*, 627–640.

Chen, C.-L., Hsieh, Y.-T., and Chen, H.-C. (2007). Phosphorylation of adducin by protein kinase Cdelta promotes cell motility. J. Cell Sci. *120*, 1157–1167.

Cooper, J.A., Walker, S.B., and Pollard, T.D. (1983). Pyrene actin: Documentation of the validity of a sensitive assay for actin polymerization. J. Muscle Res. Cell Motil. *4*, 253–262.

Coyle, I.P., Koh, Y.-H., Lee, W.-C.M., Slind, J., Fergestad, T., Littleton, J.T., and Ganetzky, B. (2004). Nervous wreck, an SH3 adaptor protein that interacts with Wsp, regulates synaptic growth in *Drosophila*. Neuron *41*, 521–534.

Datwani, A., McConnell, M.J., Kanold, P.O., Micheva, K.D., Busse, B., Shamloo, M., Smith, S.J., and Shatz, C.J. (2009). Classical MHCI molecules regulate retinogeniculate refinement and limit ocular dominance plasticity. Neuron *64*, 463–470.

DiAntonio, A., Haghighi, A.P., Portman, S.L., Lee, J.D., Amaranto, A.M., and Goodman, C.S. (2001). Ubiquitination-dependent mechanisms regulate synaptic growth and function. Nature *412*, 449–452.

Dietzl, G., Chen, D., Schnorrer, F., Su, K.C., Barinova, Y., Fellner, M., Gasser, B., Kinsey, K., Oppel, S., Scheiblauer, S., et al. (2007). A genome-wide transgenic RNAi library for conditional gene inactivation in Drosophila. Nature *448*, 151–156.

Dutta, D., Bloor, J.W., Ruiz-Gomez, M., VijayRaghavan, K., and Kiehart, D.P. (2002). Real-time imaging of morphogenetic movements in Drosophila using Gal4-UAS-driven expression of GFP fused to the actin-binding domain of moesin. Genesis *34*, 146–151.

Eaton, B.A., and Davis, G.W. (2005). LIM Kinase1 controls synaptic stability downstream of the type II BMP receptor. Neuron *47*, 695–708.

Eaton, B.A., Fetter, R.D., and Davis, G.W. (2002). Dynactin is necessary for synapse stabilization. Neuron *34*, 729–741.

Fukata, Y., Oshiro, N., Kinoshita, N., Kawano, Y., Matsuoka, Y., Bennett, V., Matsuura, Y., and Kaibuchi, K. (1999). Phosphorylation of adducin by Rho-kinase plays a crucial role in cell motility. J. Cell Biol. *145*, 347–361.

Goda, Y., and Davis, G.W. (2003). Mechanisms of synapse assembly and disassembly. Neuron *40*, 243–264.

Gordon, D.J., Eisenberg, E., and Korn, E.D. (1976). Characterization of cytoplasmic actin isolated from Acanthamoeba castellanii by a new method. J. Biol. Chem. *251*, 4778–4786.

Gruenbaum, L.M., Gilligan, D.M., Picciotto, M.R., Marinesco, S., and Carew, T.J. (2003). Identification and characterization of Aplysia adducin, an Aplysia cytoskeletal protein homologous to mammalian adducins: Increased phosphorylation at a protein kinase C consensus site during long-term synaptic facilitation. J. Neurosci. *23*, 2675–2685.

Holtmaat, A., and Svoboda, K. (2009). Experience-dependent structural synaptic plasticity in the mammalian brain. Nat. Rev. Neurosci. *10*, 647–658.

Huang, E.J., and Reichardt, L.F. (2001). Neurotrophins: Roles in neuronal development and function. Annu. Rev. Neurosci. *24*, 677–736.

Iwasa, J.H., and Mullins, R.D. (2007). Spatial and temporal relationships between actin-filament nucleation, capping, and disassembly. Curr. Biol. *17*, 395–406.

Kittel, R.J., Wichmann, C., Rasse, T.M., Fouquet, W., Schmidt, M., Schmid, A., Wagh, D.A., Pawlu, C., Kellner, R.R., Willig, K.I., et al. (2006). Bruchpilot promotes active zone assembly, Ca^{2+} channel clustering, and vesicle release. Science *312*, 1051–1054.

Koch, I., Schwarz, H., Beuchle, D., Goellner, B., Langegger, M., and Aberle, H. (2008). *Drosophila* ankyrin 2 is required for synaptic stability. Neuron *58*, 210–222.

Koh, T.-W., Verstreken, P., and Bellen, H.J. (2004). Dap160/intersectin acts as a stabilizing scaffold required for synaptic development and vesicle endocytosis. Neuron *43*, 193–205.

Kuhlman, P.A., Hughes, C.A., Bennett, V., and Fowler, V.M. (1996). A new function for adducin. Calcium/calmodulin-regulated capping of the barbed ends of actin filaments. J. Biol. Chem. *271*, 7986–7991.

Li, X., Matsuoka, Y., and Bennett, V. (1998). Adducin preferentially recruits spectrin to the fast growing ends of actin filaments in a complex requiring the MARCKS-related domain and a newly defined oligomerization domain. J. Biol. Chem. *273*, 19329–19338.

Luo, L. (2002). Actin cytoskeleton regulation in neuronal morphogenesis and structural plasticity. Annu. Rev. Cell Dev. Biol. *18*, 601–635.

Luo, L., and O'Leary, D.D.M. (2005). Axon retraction and degeneration in development and disease. Annu. Rev. Neurosci. *28*, 127–156.

Marie, B., Sweeney, S.T., Poskanzer, K.E., Roos, J., Kelly, R.B., and Davis, G.W. (2004). Dap160/intersectin scaffolds the periactive zone to achieve high-fidelity endocytosis and normal synaptic growth. Neuron *43*, 207–219.

Marrus, S.B., Portman, S.L., Allen, M.J., Moffat, K.G., and DiAntonio, A. (2004). Differential localization of glutamate receptor subunits at the Drosophila neuromuscular junction. J. Neurosci. *24*, 1406–1415.

Massaro, C.M., Pielage, J., and Davis, G.W. (2009). Molecular mechanisms that enhance synapse stability despite persistent disruption of the spectrin/ankyrin/microtubule cytoskeleton. J. Cell Biol. *187*, 101–117.

Matsuoka, Y., Li, X., and Bennett, V. (2000). Adducin: Structure, function and regulation. Cell. Mol. Life Sci. *57*, 884–895.

Mejillano, M.R., Kojima, S., Applewhite, D.A., Gertler, F.B., Svitkina, T.M., and Borisy, G.G. (2004). Lamellipodial versus filopodial mode of the actin nanomachinery: Pivotal role of the filament barbed end. Cell *118*, 363–373.

Menna, E., Disanza, A., Cagnoli, C., Schenk, U., Gelsomino, G., Frittoli, E., Hertzog, M., Offenhauser, N., Sawallisch, C., Kreienkamp, H.-J., et al. (2009). Eps8 regulates axonal filopodia in hippocampal neurons in response to brain-derived neurotrophic factor (BDNF). PLoS Biol. *7*, e1000138.

Nikolaev, A., McLaughlin, T., O'Leary, D.D.M., and Tessier-Lavigne, M. (2009). APP binds DR6 to trigger axon pruning and neuron death via distinct caspases. Nature *457*, 981–989.

Nunes, P., Haines, N., Kuppuswamy, V., Fleet, D.J., and Stewart, B.A. (2006). Synaptic vesicle mobility and presynaptic F-actin are disrupted in a N-ethylmaleimide-sensitive factor allele of Drosophila. Mol. Biol. Cell *17*, 4709–4719.

Pariser, H., Herradon, G., Ezquerra, L., Perez-Pinera, P., and Deuel, T.F. (2005). Pleiotrophin regulates serine phosphorylation and the cellular distribution of beta-adducin through activation of protein kinase C. Proc. Natl. Acad. Sci. USA *102*, 12407–12412.

Petrella, L.N., Smith-Leiker, T., and Cooley, L. (2007). The Ovhts polyprotein is cleaved to produce fusome and ring canal proteins required for Drosophila oogenesis. Development *134*, 703–712.

Pielage, J., Fetter, R.D., and Davis, G.W. (2005). Presynaptic spectrin is essential for synapse stabilization. Curr. Biol. *15*, 918–928.

Pielage, J., Fetter, R.D., and Davis, G.W. (2006). A postsynaptic spectrin scaffold defines active zone size, spacing, and efficacy at the Drosophila neuromuscular junction. J. Cell Biol. *175*, 491–503.

Pielage, J., Cheng, L., Fetter, R.D., Carlton, P.M., Sedat, J.W., and Davis, G.W. (2008). A presynaptic giant ankyrin stabilizes the NMJ through regulation of presynaptic microtubules and transsynaptic cell adhesion. Neuron *58*, 195–209.

Porro, F., Rosato-Siri, M., Leone, E., Costessi, L., Iaconcig, A., Tongiorgi, E., and Muro, A.F. (2010). beta-adducin (Add2) KO mice show synaptic plasticity, motor coordination and behavioral deficits accompanied by changes in the expression and phosphorylation levels of the alpha- and gamma-adducin subunits. Genes Brain Behav. *9*, 84–96.

Rabenstein, R.L., Addy, N.A., Caldarone, B.J., Asaka, Y., Gruenbaum, L.M., Peters, L.L., Gilligan, D.M., Fitzsimonds, R.M., and Picciotto, M.R. (2005). Impaired synaptic plasticity and learning in mice lacking beta-adducin, an actin-regulating protein. J. Neurosci. *25*, 2138–2145.

Rasse, T.M., Fouquet, W., Schmid, A., Kittel, R.J., Mertel, S., Sigrist, C.B., Schmidt, M., Guzman, A., Merino, C., Qin, G., et al. (2005). Glutamate receptor dynamics organizing synapse formation in vivo. Nat. Neurosci. *8*, 898–905.

Robinson, D.N., Cant, K., and Cooley, L. (1994). Morphogenesis of Drosophila ovarian ring canals. Development *120*, 2015–2025.

Roos, J., Hummel, T., Ng, N., Klämbt, C., and Davis, G.W. (2000). *Drosophila* Futsch regulates synaptic microtubule organization and is necessary for synaptic growth. Neuron *26*, 371–382.

Seidel, B., Zuschratter, W., Wex, H., Garner, C.C., and Gundelfinger, E.D. (1995). Spatial and sub-cellular localization of the membrane cytoskeleton-associated protein alpha-adducin in the rat brain. Brain Res. *700*, 13–24.

Sweeney, S.T., and Davis, G.W. (2002). Unrestricted synaptic growth in spinster-a late endosomal protein implicated in TGF-beta-mediated synaptic growth regulation. Neuron *36*, 403–416.

van der Gucht, J., Paluch, E., Plastino, J., and Sykes, C. (2005). Stress release drives symmetry breaking for actin-based movement. Proc. Natl. Acad. Sci. USA *102*, 7847–7852.

Venken, K.J.T., and Bellen, H.J. (2007). Transgenesis upgrades for Drosophila melanogaster. Development *134*, 3571–3584.

Wagh, D.A., Rasse, T.M., Asan, E., Hofbauer, A., Schwenkert, I., Dürrbeck, H., Buchner, S., Dabauvalle, M.-C., Schmidt, M., Qin, G., et al. (2006). Bruchpilot, a protein with homology to ELKS/CAST, is required for structural integrity and function of synaptic active zones in *Drosophila*. Neuron *49*, 833–844.

Walsh, M.K., and Lichtman, J.W. (2003). In vivo time-lapse imaging of synaptic takeover associated with naturally occurring synapse elimination. Neuron *37*, 67–73.

Wan, H.I., DiAntonio, A., Fetter, R.D., Bergstrom, K., Strauss, R., and Goodman, C.S. (2000). Highwire regulates synaptic growth in Drosophila. Neuron *26*, 313–329.

Watts, R.J., Hoopfer, E.D., and Luo, L. (2003). Axon pruning during *Drosophila* metamorphosis: Evidence for local degeneration and requirement of the ubiquitin-proteasome system. Neuron *38*, 871–885.

Xu, T., Yu, X., Perlik, A., Tobin, W., Zweig, J., Tennant, K., Jones, T., and Zuo, Y. (2009). Rapid formation and selective stabilization of synapses for enduring motor memories. Nature *462*, 915–919.

Yue, L., and Spradling, A.C. (1992). hu-li tai shao, a gene required for ring canal formation during Drosophila oogenesis, encodes a homolog of adducin. Genes Dev. *6* (12B), 2443–2454.

Zaccai, M., and Lipshitz, H.D. (1996). Differential distributions of two adducin-like protein isoforms in the Drosophila ovary and early embryo. Zygote *4*, 159–166.

Zuchero, J.B., Coutts, A.S., Quinlan, M.E., Thangue, N.B.L., and Mullins, R.D. (2009). p53-cofactor JMY is a multifunctional actin nucleation factor. Nat. Cell Biol. *11*, 451–459.